LModeA-nano: A PyMOL Plugin for Calculating Bond Strength in Solids, Surfaces, and Molecules via Local Vibrational Mode Analysis

Yunwen Tao,* Wenli Zou, Sadisha Nanayakkara, and Elfi Kraka*

Read Online

| ACCESS | 📊 Metrics & More | 📄 Article Recommendations | 🆅 Supporting Information |

ABSTRACT: The analysis of chemical bonding in crystal structures and surfaces is an important research topic in theoretical chemistry. In this work, we present a PyMOL plugin, named LModeA-nano, as implementation of the local vibrational mode theory for periodic systems (Tao et al. *J. Chem. Theory Comput.* **2019**, *15*, 1761) assessing bond strength in terms of local stretching force constants in extended systems of one, two, and three dimensions. LModeA-nano can also analyze chemical bonds in isolated molecular systems thus enabling a head-to-head comparison of bond strength across systems with different dimensions in periodicity (0−3D). The new code is interfaced to the output generated by various solid-state modeling packages including VASP, CP2K, Quantum ESPRESSO, CASTEP, and CRYSTAL. LModeA-nano is cross-platform, open-source and freely available on GitHub: https://github.com/smutao/LModeA-nano.
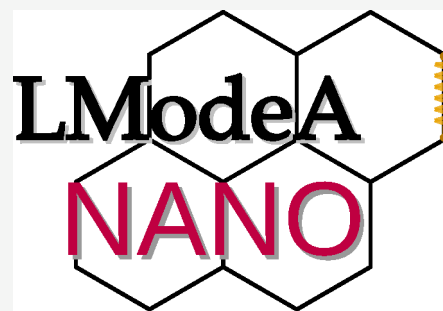
1. INTRODUCTION

Chemical bonding describing the physical forces between atoms in molecules and solids is one of the most important concepts in chemistry.[1−7] While the theoretical study on chemical bonds was started by Pauling from the molecular structures,[8] understanding the chemical bonding properties in periodic solid-state structures is equally essential because the chemical bonds at the microscopic level determine the macroscopic properties of the solids.

Thanks to the rapid development in the field of computational chemistry and ever increasing performance of computers in the past decades, the atomistic modeling of solid-state materials at the quantum mechanical level is able to provide the energy, structure, and various spectroscopic properties at good accuracy supporting the *in silico* design of novel materials. It also offers various theoretical tools to study chemical bonding in solids and surfaces. In the following, we briefly summarize some selected solid-state modeling packages and third-party postprocessing packages as listed in Table 1, providing a short discussion from the perspective of the bonding analysis methods implemented in these software packages.

1.1. ELF in Most Solid-State Modeling Packages. The electron localization function (ELF) is the most widely supported analysis in many solid-state modeling packages. It was introduced by Becke and Edgecombe in 1990 as a measure of electron localization in space ranging from 0 to 1.[9] A larger ELF value indicates a covalent bond, a lone pair, or inner shells of an atom. The representation of ELF in the form of an isosurface map can graphically display the presence of lone pairs and covalent bonds.

1.2. Quantum ESPRESSO. Besides ELF, Quantum ESPRESSO (QE)[10] supports the bonding analysis by means of reduced density gradient (RDG) and density overlap regions indicator (DORI). The RDG method also known as noncovalent interaction (NCI) analysis was developed by Yang and co-workers in 2010 to study weak interactions.[11] It allows for visualization of the region of noncovalent interactions in 3D space and also indicates the presence of these interactions via the spikes in RDG vs electron density ρ plots. In addition, the strength and type of the interaction can be obtained by mapping $sign(\lambda_2) \cdot \rho$ onto RDG isosurfaces (λ_2 is the second largest eigenvalue of Hessian of electron density).[12] Three types of interactions can be differentiated including strong attraction (e.g., hydrogen bonding), weak van der Waals interaction, and strong repulsion (e.g., steric effect). DORI as a function of electron density ρ was proposed by Silva and Corminboeuf in 2014.[13] The main feature of DORI is the simultaneous visualization of covalent bonds and noncovalent interactions with a single real-space function.

1.3. CRYSTAL17. The TOPOND module in the CRYSTAL17 package[14] performs the topological analysis of the electron density under the framework of Bader's quantum theory of atoms in molecules (QTAIM).[15,16] The topological analysis partitions the electron density in a molecule or solid

Table 1. List of Available Programs for Chemical Bonding Analysis in Solids

program	type of analysis	bond types[a]	molecule[b]	cost[c]	platform
		Solid-State Modeling Packages			
most packages[d]	ELF	C.B.	yes	t_{sp}	
QE	DORI/RDG	any/N.C.	yes	t_{sp}	Linux, Mac
CRYSTAL17	QTAIM	any	yes	t_{sp}	Linux
	COHP/COOP	C.B.	no*		
BAND	pEDA	any	yes	$3t_{sp}$	all
		Third-Party Packages			
CrystalExplorer	Hirshfeld surface analysis	N.C.	no*	trivial	all
LOBSTER	COHP/COOP	C.B.	yes	t_{sp}	all
Periodic NBO	NBO	any	separate	t_{sp}	Linux, Mac
ssAdNDP	AdNDP	C.B.	separate	t_{sp}	Linux, Mac
critic2	QTAIM/ELF/RDG	any/C.B./N.C.	yes	t_{sp}	Linux, Mac
AIM-UC	QTAIM	any	yes	t_{sp}	Linux, Win
TopChem2	QTAIM/ELF	any/C.B.	yes	t_{sp}	Linux
Multiwfn	QTAIM	any	yes	t_{sp}	all
	RDG	N.C.		trivial$-t_{sp}$	
	IGM/IGMH	any		trivial/t_{sp}	
	DORI/IRI	any		t_{sp}	
	bond orders	C.B.		t_{sp}	
LModeA-nano (this work)	local mode analysis	any	yes[e]	$6n \cdot t_{sp}^{f}$	all

[a]Type of chemical bonding which can be analyzed with this method. C.B. and N.C. are abbreviations for chemical bond and noncovalent interactions, respectively. C.B. includes covalent, ionic, and metallic bonds, while N.C. is the intermolecular interaction. [b]This column indicates whether the supported analysis in the program can be directly applied to isolated molecular systems or a separate program is available for molecules. [c]Computational cost for the analysis starting from the crystal structure. t_{sp} is the computational time for the single-point energy calculation at the DFT level. t_{sp}^{f} is the time for the single-point energy and force evaluation calculation at the DFT level. n is the number of atoms in the primitive cell. [d]The list includes but is not limited to VASP, Quantum ESPRESSO, CP2K, CASTEP, and DMol3. [e]A separate program LModeA is also available for molecular systems.[40]

into basins associated with atoms, and two neighboring basins are separated by the so-called zero-flux surfaces. Two atoms are considered as bonded if there exists one $(3, -1)$ bond critical point on the interbasin surface. Real-space functions like electron density, Laplacian of density, Hessian eigenvalues of the density, and various energy densities[17] can be calculated on bond critical points as the properties of the bond of interest. The crystal orbital overlap population (COOP) method developed by Hoffman and Hughbanks in 1983[18] projects single atomic orbitals onto crystalline orbitals related to two bonded atoms or fragments A and B, and then this density of states (DOS) is weighted by the overlap matrix. In this way, the electron density is partitioned into bonding, nonbonding, and antibonding regions. The crystal orbital Hamilton population (COHP) method developed by Dronskowski and Blöchl in 1993[19] is slightly different in the sense that the above-mentioned DOS is weighted by the Hamiltonian matrix leading to the partitioning of the band structure energy into bonding, nonbonding, and antibonding contributions. Both COOP and COHP have opposite signs for bonding and antibonding characters. In the CRYSTAL17 program, the COHP/COOP analysis is also applicable to molecules with some workarounds.[20]

1.4. BAND. The periodic energy decomposition analysis (pEDA)[21] implemented in the BAND package (http://www.scm.com/) was developed by Raupach and Tonner in 2015 as a theoretical extension of the energy decomposition analysis (EDA) for molecules with various implementations.[22,23] pEDA decomposes the bonding energy between two fragments into specific types of energy contributions. It is especially useful for the analysis of the surface–adsorbate interactions and other two-body situations.

1.5. CrystalExplorer. The Hirshfeld surface analysis implemented in the CrystalExplorer program[24] is widely used among chemists to visualize intermolecular interactions in molecular crystals. This method which was originally developed by Spackman and Byrom in 1997 defines the Hirshfeld weight $w(r)$ by summing up the promolecular density of atoms in a molecule divided by the sum of the promolecular density of the atoms in the whole crystal.[25] The Hirshfeld surface for the molecule of interest is then defined by the isosurface $w(\mathbf{r}) = 0.5$. By mapping various properties derived from distance and density onto the Hirshfeld surface, the presence of intermolecular interactions concerning the selected molecular fragment can be vividly demonstrated. In addition, the fingerprint plot based on two carefully selected distances reveals the existence of intermolecular interactions, so that the 3D surface can be represented in a 2D format.[26] The recent version of CrystalExplorer also supports the calculation of model interaction energies between two fragments calculated with relatively low-level *ab initio* methods. CrystalExplorer does not natively support the analysis of molecular clusters unless the molecular structure is prepared in the `CIF` format.

1.6. LOBSTER. The COHP/COOP implementation in the LOBSTER program[27] differs from the one in the CRYSTAL17 program in the way that the former takes the delocalized plane-waves as the input wave function instead of the localized atom-centered one. To accommodate this, a built-in Slater type basis set is projected to the delocalized crystalline orbitals. One important quantity accessible in the LOBSTER program is the integrated value of COHP (ICOHP) which can be used as an approximate bond energy.

1.7. Periodic NBO. The natural bond orbital (NBO) analysis introduced by by Weinhold for molecular systems[28,29]

was generalized to periodic systems by Dunnington and Schmidt in 2012.[30] The NBO method extracts from the delocalized molecular/crystal orbitals the localized orbitals based on the density matrix providing a Lewis-like description of bonding.

1.8. SSAdNDP. The adaptive natural density partitioning (AdNDP) method introduced by Zubarev and Boldyrev in 2008[31] is a theoretical extension of the NBO method aiming to describe both localized (two-centered Lewis-type) and multi-centered bonds. Schmidt, Boldyrev, and co-workers generalized this method to periodic systems in 2013.[32]

1.9. critic2, AIM-UC, and TopChem2. These three programs feature the topological analysis based on Bader's QTAIM framework, and some of them also support ELF and RDG analyses.[33−35]

1.10. Multiwfn. Apart from the above-mentioned chemical bonding analysis methods including QTAIM, RDG, and DORI, the Multiwfn program[36] supports additional new features. The independent gradient model (IGM) introduced by Hénon and co-workers in 2017[37] is similar to the DORI function in visualizing the interfragment and intrafragment interactions, but IGM can show these two interactions separately while DORI cannot. Its original version based on promolecular density only needs the Cartesian coordinates of a molecule or solid as the input. On this basis, Lu proposed an improved version called IGMH (IGM analysis based on Hirshfeld partition of molecular density) which provides better graphical effect and more rigorous physical meaning than the original implementation.[38] The recently introduced interaction region indicator (IRI) method by Lu and Chen[39] is an alternative to DORI and IGM in showing both the chemical bonding and weak interactions. It is based on a minor modification of the formula of RDG and could also classify the noncovalent interactions into three categories with $sign(\lambda_2) \cdot \rho$ as RDG does. In addition, Multiwfn can also calculate Mayer bond order, multicenter bond order, Wiberg bond order, and Mulliken bond order in solids. Unlike the programs discussed above, Multiwfn does not consider the k-point sampling and therefore requires a large supercell as a workaround if the wave function is provided as input data. For analyses independent of the wave function information, such limitation is lifted.

Recently, we developed the local vibrational mode theory for periodic systems as a theoretical extension of the original theory for isolated molecules.[41] The new theory enables the determination of the intrinsic strength of any chemical bond in periodic systems of one through three dimensions via local stretching force constants. Most importantly, the force constants calculated for periodic systems can be directly compared with the ones for isolated molecules due to the solid physical foundation on vibrational spectroscopy.[40] Noteworthy is that the chemical bond strength is often assessed via the bond (dissociation) energy for covalent bonds and binding energy for noncovalent interactions. However, the straightforward calculation of such energy-based bond strength in complex systems, e.g., large molecular clusters or cocrystals, is challenging. In recent years, the local stretching force constant (also known as relaxed force constant) is gradually being accepted by the community as a generally applicable bond strength measure.[42]

It is worth noting that the force constant has already been used by chemists to quantify and compare chemical bond strengths in solids in seven different ways since the 1950s as follows. (I) While the phonon mode concerning the chemical bond of interest is highly localized, the equation of the classical vibrational mode is used to calculate force constant k from the vibrational frequency ν which can be either experimentally measured or calculated

$$\nu = \frac{1}{2\pi c} \sqrt{\frac{k}{\mu}} \tag{1}$$

where μ is the reduced mass of the bonded atom pair A−B.[43−56]

$$\mu = \frac{M_A M_B}{M_A + M_B} \tag{2}$$

This method is useful when experimental vibrational spectra are available; however, it has limited applicability because vibrational modes are in general delocalized.[57,58] (II) A closely related approach is to employ the force field models consisting of force constant parameters that can best reproduce experimentally measured vibrational frequencies, and then the refined force constant values of chemical bonds are directly used as bond strength descriptors.[59−61] This method is feasible for simple solid structures because only a few parameters are needed, but for complicated structures, the parameter optimization becomes rather difficult. In addition, this force field based method to calculate vibrational spectra has become obsolete due to the availability of DFT methods in calculating the lattice vibrations.[62] (III) For some simple solid structures, force constants of chemical bonds can be calculated from empirical equations related to properties like effective nuclear charge, bond length, lattice energy, Madelung constant, and so forth.[63−71] (IV) For certain types of lattice structures (especially 2D materials), there exist analytical expressions between the bond stretching force constant and elastic properties (e.g., bulk modulus, Young's modulus, and elastic constant).[72−77] (V) With the advent of the phonon calculation at the DFT level, one possible way to calculate the mean force constant $\langle k \rangle$ of the chemical bonds centered around one atom in solid is via

$$\langle k \rangle = \frac{M}{\hbar^2} \int_0^\infty g(E)E^2 dE \tag{3}$$

where $g(E)$ is the partial phonon density of states (PDOS) for the central atom, and E is the vibrational energy.[78−81] (VI) One commonly used computational method to get the force constant of a bond is to project the 3×3 matrix $\mathbf{f}_{AB}$ collecting the force constants between two bonding atoms (A and B) into the direction parallel to this bond[82−92]

$$k = \mathbf{u}\mathbf{f}_{AB}\mathbf{u}^T \tag{4}$$

where

$$\mathbf{f}_{AB} = \begin{bmatrix} f_{AB}^{xx} & f_{AB}^{xy} & f_{AB}^{xz} \\ f_{AB}^{yx} & f_{AB}^{yy} & f_{AB}^{yz} \\ f_{AB}^{zx} & f_{AB}^{zy} & f_{AB}^{zz} \end{bmatrix} \tag{5}$$

$$\mathbf{u} = \frac{\mathbf{r}_A - \mathbf{r}_B}{|\mathbf{r}_A - \mathbf{r}_B|} \tag{6}$$

$\mathbf{r}_A$ and $\mathbf{r}_B$ are the Cartesian coordinates of two bonded atoms. This method appears intuitively reasonable because the matrix $\mathbf{f}_{AB}$ indeed quantifies the real-space physical interaction between atoms A and B; however, $\mathbf{f}_{AB}$ is simply an off-diagonal

block of the full Hessian matrix $\mathbf{f}^x$ (in Cartesian coordinates), while the diagonal blocks for atoms A and B are discarded. Therefore, this approach is missing a solid physical basis. (VII) Another straightforward computational method to get the stretching force constant for bond A−B in a solid is applying the second-order finite difference to the total potential energy U with regard to the bond length r based on the optimized structure

$$k \approx \frac{U(r_0 + \Delta r) - 2U(r_0) + U(r_0 - \Delta r)}{\Delta r^2} \qquad (7)$$

so that the stretching force constant k is the curvature of a fitted quadratic function from the harmonic approximation of the potential energy surface.[93−95] This method is easy to implement, and the corresponding *rigid* force constant k is a good approximation to the local mode force constant k_n^a (i.e., relaxed force constant) defined in the local vibrational mode theory. However, this rigid stretching force constant k overlooks the relaxation of other atoms to the infinitesimal displacement Δr in the bond A−B and is thus slightly larger than the local stretching force constant k_n^a.[96−98]

In this work, we introduce LModeA-nano as a PyMOL plugin for calculating the local stretching force constants of chemical bonds in periodic solid-state systems as well as molecular systems. The paper is structured in the following way: First, the local vibrational mode theory and its key equations are summarized. Then, the architecture of the LModeA-nano code and different routes to obtain the Hessian matrix in Cartesian coordinates from molecular/solid-state modeling packages are illustrated. Three different showcase examples are elaborated to demonstrate the application of the local vibrational mode theory in quantifying and comparing chemical bond strength. The conclusions, following some remarks on local stretching force constants, are given in two sections. The computational details for the showcase examples are given in the last section.

2. LOCAL VIBRATIONAL MODE THEORY

The local vibrational mode theory was originally developed by Konkoli and Cremer in 1998 to describe the adiabatic internal modes (later known as *local vibrational modes*) associated with internal coordinates (e.g., bond length, bond angle, etc.) in molecules based on the harmonic normal mode vibrations.[99−102] A local vibrational mode associated with the internal coordinate q_n in a molecule is defined as the motion of an infinitesimal change in this internal coordinate followed by the relaxation of all other parts of this molecule.[40,103]

In 2019, we extended the local vibrational mode theory to periodic systems with one, two, and three dimensions.[41] The corresponding local vibrational mode is defined as the motion of an infinitesimal change in an internal coordinate q_n within the primitive unit cell followed by the relaxation of other atoms in this cell, and such motion is synchronized in all primitive cells. This theoretical extension is based upon the phonons of the periodic systems at the Γ point ($\mathbf{q} = (0, 0, 0)$) where the phonon frequencies can be experimentally measured by infrared or/and Raman spectroscopy. As a result, the definition of a local vibrational mode is valid in most periodic systems except the bulk metals (e.g., copper, gold, and aluminum) whose primitive cells contain only one atom leading to zero phonon frequencies at the Γ point.

The detailed derivation of local vibrational mode theory starting from the Wilson equation of vibrational spectroscopy[57] or Euler−Lagrange equation have been introduced in our previous work.[40] In the following, we briefly summarize the unified formulation to calculate the force constants and frequencies of local vibrational modes in both molecular and periodic systems.

For an N-atom molecular structure optimized to a local minimum point on the potential energy landscape or an optimized primitive cell structure having N atoms, its Hessian matrix $\mathbf{f}^x$ (containing the second-order energy derivatives with regard to Cartesian coordinates) in the dimension of $3N \times 3N$ has N_{vib} nonzero eigenvalues collected in the diagonal matrix $\mathbf{\Lambda}$

$$\mathbf{f}^x \mathbf{C} = \mathbf{C} \mathbf{\Lambda} \qquad (8)$$

where N_{vib} is $3N − 5$ or $3N − 6$ for linear or nonlinear molecular systems, respectively. For periodic systems, N_{vib} takes the value of $3N − 4$ for one-dimensional systems or $3N − 3$ for two-/three-dimensional systems. Matrix $\mathbf{C}$ collects N_{vib} eigenvectors columnwise.

Eq 8 can be rewritten as

$$\mathbf{\Lambda} = \mathbf{C}^T \mathbf{f}^x \mathbf{C} \qquad (9)$$

where superscript T represents the matrix transpose.

The local vibrational mode associated with an internal coordinate q_n needs the evaluation of the Wilson $\mathbf{B}$-matrix,[57,104] which is the partial derivatives of q_n with respect to the Cartesian coordinates

$$\mathbf{b}_n = \frac{\partial q_n}{\partial \mathbf{x}} \qquad (10)$$

Then, the vector $\mathbf{d}_n = \mathbf{b}_n \mathbf{C}$ is used to calculate the local mode force constant k_n^a via

$$k_n^a = (\mathbf{d}_n (\mathbf{\Lambda})^{-1} \mathbf{d}_n^T)^{-1} \qquad (11)$$

The local mode force constant k_n^a of internal coordinate q_n was originally named the *adiabatic force constant*,[99] where the superscript a (adiabatic) means "relaxed", and the subscript n stands for this internal coordinate parameter q_n. It is also the curvature of the potential energy surface (PES) in the direction of this internal coordinate as the leading parameter. When the internal coordinate specifies a bond length, the corresponding local stretching force constant usually takes the unit of mdyn/Å (1 mdyn/Å = 1 N/cm = 100 N/m).

The local vibrational frequency ω_n^a can be derived with the help of the Wilson $\mathbf{G}$-matrix

$$(\omega_n^a)^2 = \frac{1}{4\pi^2 c^2} k_n^a G_{nn} \qquad (12)$$

where the diagonal element G_{nn} corresponds to the reduced mass associated with $\mathbf{b}_n$. Noteworthy is that the local vibrational mode frequencies cannot be directly measured with vibrational spectroscopy like for molecular vibrations and phonons in solids. However, the adiabatic connection scheme (ACS) method is able to establish a one-to-one correlation between a complete nonredundant set of local vibrational modes and the normal vibrational modes in molecular systems.[103] This method is definitely possible to be extended to periodic systems.

Unlike the local vibrational frequency ω_n^a which is dependent on the mass of atoms involved in the internal coordinate q_n of interest, the local mode force constant k_n^a is mass-independent

and reflects the pure electronic factors. This qualifies the local stretching force constant as a unique bond strength descriptor. Our efforts in utilizing the local stretching force constant to measure intrinsic strength of covalent bonds and various noncovalent interactions (e.g., hydrogen, halogen, pnicogen, chalcogen, and tetrel bonding) were summarized in a recent review paper.[40]

Apart from the above-mentioned procedure to calculate local mode force constants based on the calculation of the full Hessian matrix $\mathbf{f}^x$, there exists a simple approach according to the physical picture of local vibrational modes. For a given chemical bond in a fully optimized molecular or primitive cell structure, we record the total potential energy as $U(r_0)$. Then, we introduce small displacements $\pm \Delta r$ (e.g., 0.005 Å) to the bond of interest and relax all other atoms (as well as the cell parameters for periodic systems); such constrained optimization results in two additional potential energy values $U(r_0 - \Delta r)$ and $U(r_0 + \Delta r)$. By applying eq 7, the local stretching force constant of this chemical bond can be calculated numerically, and this result is equivalent to the force constant calculated with the full Hessian. In addition, this simplified approach is computationally more efficient for large systems where the evaluation of the full Hessian can be expensive.

3. CODE STRUCTURE AND GENERAL WORKFLOW

In this work, we have implemented the local vibrational mode theory for both periodic and isolated molecular systems in a PyMOL plugin named LModeA-nano. This new code emphasizing the periodic systems is a descendant of our recently released LModeA program.[40] The LModeA code was developed for local vibrational mode analysis in molecular systems, and it supports features including (1) adiabatic connection scheme,[103] (2) normal mode decomposition,[101,102] and (3) correction of Hessian matrix based on experimental vibrational frequencies.[105]

As shown in Figure 1, LModeA-nano takes the optimized primitive cell/molecular structure and its Hessian matrix as the input data and then calculates local mode force constants and frequencies as the output. LModeA-nano is composed of the following parts:

- The PyMOL program originally developed by DeLano and now maintained by Schrödinger, Inc. was employed as the foundation of our code.[106,107] It is one of the most popular molecular visualization packages and provides Python interfaces allowing researchers to develop their own plugins utilizing this powerful platform.

- The codebase written in Python language can (1) communicate with PyMOL via interfaces, (2) parse input data generated by various solid-state/quantum chemistry modeling packages, (3) calculate the local mode force constants and frequencies, and (4) save the calculated results on disks.

- The graphical user interface (GUI) window allows the users to load the input data for local vibrational mode analysis, and it temporarily holds the calculation results in a table region. A snapshot of the GUI window is shown in Supporting Information Figure S1.

- The wizard as part of the codebase assists the user to specify the internal coordinate (e.g., bond and angle) for the local vibrational mode analysis by selecting certain atoms in the molecular/solid structure.
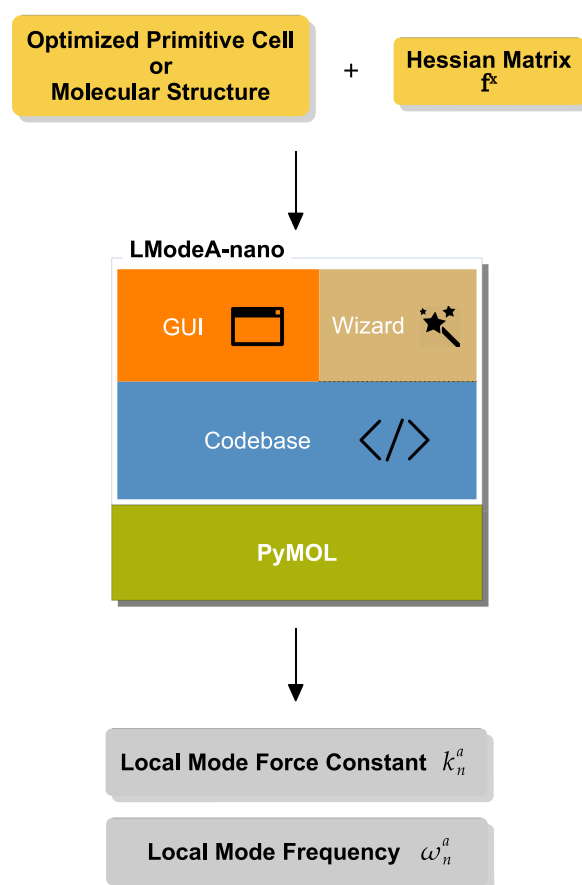

Figure 1. Flowchart for the LModeA-nano as a PyMOL plugin.

For the local vibrational mode analysis, the most critical input data is the Hessian matrix $\mathbf{f}^x$ collecting the second-order energy derivatives with regard to Cartesian coordinates of the optimized molecular/solid structure. LModeA-nano is able to extract the Hessian information from the output files generated by the solid-state modeling packages in three different ways as shown in Figure 2.

- LModeA-nano directly takes the already formatted Hessian data file generated by solid-state modeling packages.

- LModeA-nano takes the Hessian data file formatted by the Phonopy program which handles the raw output files from solid-state modeling packages. Phonopy is an open-source program developed by Togo to calculate the phonon and related properties of solids.[62]

- The Phonopy package generates the primitive cell structure with displacements starting from an optimized structure, and these perturbed structures are used for force evaluation with solid-state modeling packages. After $6N$ force evaluations (N is the number of atoms in the primitive cell), Phonopy obtains the Hessian matrix for LModeA-nano from the forces and displacements with the modified Parlinski-Li-Kawazoe method.[108,109] This approach is especially useful for computational efficiency as the force evaluation of different perturbed structures can be distributed to different computational nodes to run in parallel.[110]

For the output from the quantum chemistry modeling packages which only handle molecular systems, LModeA-nano can directly read in the Hessian data file generated by a
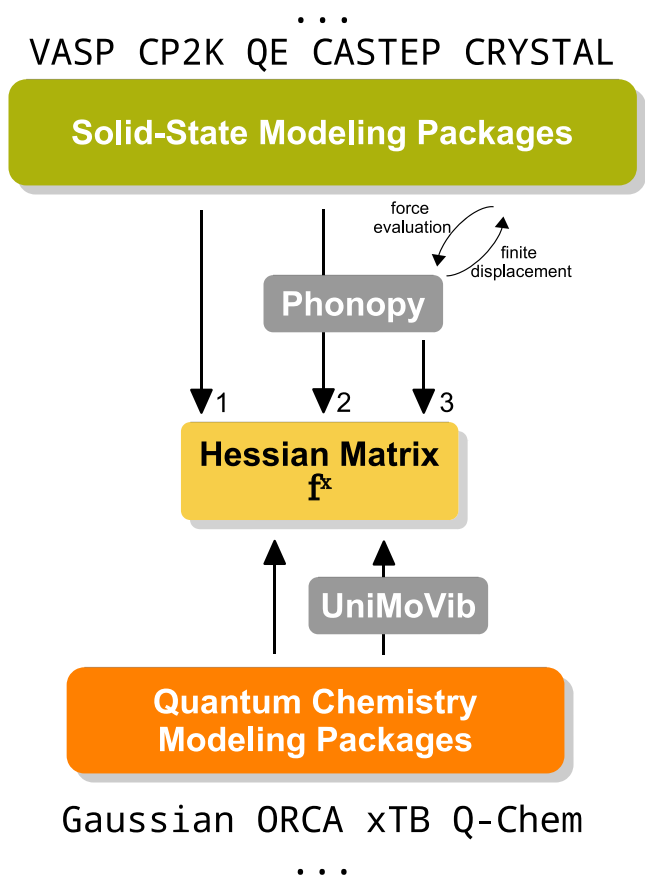
VASP CP2K QE CASTEP CRYSTAL

Solid-State Modeling Packages

Phonopy

force evaluation

finite displacement

1 2 3

Hessian Matrix
fˣ

UniMoVib

Quantum Chemistry Modeling Packages

Gaussian ORCA xTB Q-Chem

Figure 2. Flowchart for calculating the Hessian matrix f^x from the solid-state modeling packages and quantum chemistry modeling packages.

number of quantum chemistry packages (e.g., Gaussian[111] or Q-Chem[112]). However, a more generally applicable approach is to read in the formatted data file created by our UniMoVib program[113] which has been interfaced to over 30 different quantum chemistry modeling packages.

4. SHOWCASE EXAMPLES

Since its introduction in 2019, the local vibrational mode theory for periodic systems has been applied in various scenarios (see Table 2). In our original theory paper,[41] we

Table 2. Applications of the Local Vibrational Mode Theory in Periodic Systems

periodicity	systems
1D	polyacetylene, $(HF)_n$ chain
2D	graphene, water layer, melamine cyanurate
3D	diamond, acetone solids, halogen-bonded cocrystals, ice polymorphs

showcased the application in one-dimensional polyacetylenes and hydrogen fluoride chains and two-dimensional graphene, water layer, and melamine cyanurate as well as three-dimensional ice I_h and acetone solid. In a theoretical study on molecular solids, we applied the local mode analysis to measure the intrinsic strength of the X−I···O type halogen bonds (X = I or Cl) and analyzed the underlying factors affecting the halogen bond strength.[114] Recently, more than 1,800 hydrogen bonds in 16 water ice polymorphs were

investigated, and new relationships between hydrogen bond strength and local structural motifs were identified.[115]

In this work, we provide three showcase examples to emphasize (1) the comparability of the local stretching force constant for the same type of chemical bonding across systems of different dimensions (from 0D to 3D), (2) the possibility of applying the local mode analysis in surfaces and interfaces, and (3) the microscopic dissection of the elasticity of materials in terms of chemical bonds and their local stretching force constants. The following discussion is complemented by a detailed description of all the computational methods used in each showcase example as presented in section 7.

4.1. Re−H Bond of the ReH_9^{2-} Dianion in Ionic Crystals. The nonahydridorhenate dianion ReH_9^{2-} is the first coordination complex with nine ligating hydrides.[116] This dianion has a faced-tricapped trigonal prism geometry with six prism hydrogens and three cap hydrogens (see Figure 3). The structure of ReH_9^{2-} was first determined in the resolved crystal structure of K_2ReH_9 in 1964, and the dianions sit in two distinct Wyckoff positions (sites a and d) with a ratio of 1:2.[117,118] Compared with the ReH_9^{2-} dianion in the gas phase, the dianion in the K_2ReH_9 solid is stabilized by the electrostatic attraction from the potassium cations. We are interested in exploring and rationalizing the influence from the lattice structure on the Re−H bond strength. In addition, we employed an isostructural Na_2ReH_9 model by replacing the potassium atoms in K_2ReH_9 to check how different counterions affect the Re−H bond strength.

The molecular structure of the ReH_9^{2-} dianion and the primitive cell structure of K_2ReH_9/Na_2ReH_9 were optimized using the revPBE density functional.[119] As listed in Table 3, the Re−H bond length in the gas-phase dianion was underestimated by our calculation compared to the calculated values at the coupled-cluster level by Schaefer and co-workers.[120] However, our calculated Re−H bond length values match quite well with the K_2ReH_9 structure resolved with the neutron diffraction study by Bronger and co-workers.[121]

From the calculation results in Table 3, the cap Re−H bonds are in general shorter than the prism Re−H bonds. The prism Re−H bond length across three different systems is within the range of 1.700−1.706 Å, and the cap Re−H bond lengths are all within 1.675−1.678 Å except the cap Re−H bond at site d in Na_2ReH_9 (1.669 Å). The local stretching force constant of the prism Re−H bond is smaller than the cap one by 0.1 mdyn/Å for the dianion in the gas phase. In two solids, the Re−H bond is in general weaker than that in the ReH_9^{2-} dianion in the gas phase, except for the cap Re−H at site d of Na_2ReH_9. This can be explained by the virtual process of moving the ReH_9^{2-} dianion from the gas phase to the lattice of cations so that part of the electron density of ReH_9^{2-} is transferred to the cations via electrostatic interactions. We still observe that the prism Re−H bonds are weaker than the cap bonds by 0.1−0.3 mdyn/Å in two solids. Comparing the Re−H bond strengths between K_2ReH_9 and Na_2ReH_9 solids, we found the Re−H bonds are slightly stronger in the latter case. This can be explained by the higher electronegativity[122] of Na (χ = 0.93) than K (χ = 0.82) so that the sodium cation has a stronger polarization effect on the Re−H bonding electron density toward the hydrogen atoms leading to reduced bond polarity. Such an effect is similar to the vibrational Stark effect[123] which relates the bond stretching frequency to the external electric field.
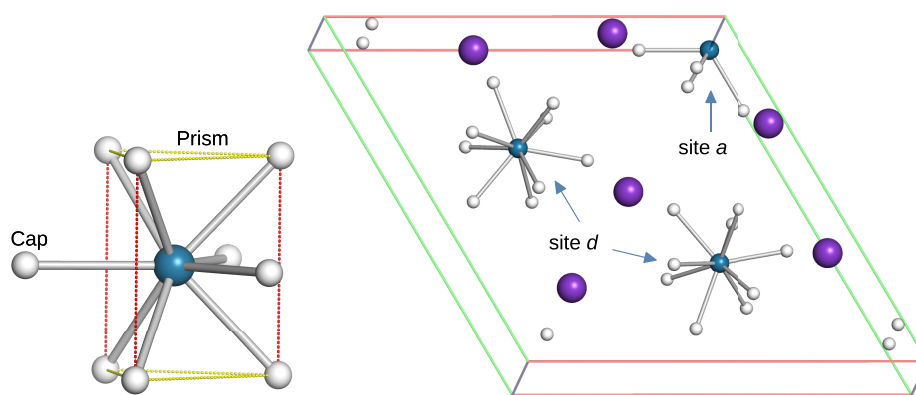
Figure 3. Molecular structure of the ReH_9^{2-} dianion (left panel) and the primitive cell structure of the K_2ReH_9 crystal (right panel). The purple balls represent the potassium cations.

Table 3. Calculated Bond Lengths and Local Stretching Force Constants/Frequencies of Re–H Bonds of the ReH_9^{2-} Dianion in the Gas Phase, K_2ReH_9, and Na_2ReH_9[a]

		prism			cap		
		r	k_n^a	ω_n^a	r	k_n^a	ω_n^a
gas phase		1.700	2.231	1943	1.677	2.328	1985
		[1.718][b]			[1.682]		
K_2ReH_9	site a	1.702	2.070	1872	1.678	2.206	1933
		[1.690][c]			[1.679]		
	site d	1.706	2.011	1845	1.676	2.242	1948
		[1.703]			[1.673]		
Na_2ReH_9	site a	1.701	2.101	1886	1.675	2.294	1970
	site d	1.703	2.073	1873	1.669	2.381	2007

[a]Units for bond length r, local stretching force constant k_n^a, and frequency ω_n^a are Å, mdyn/Å, and cm^{-1} respectively. [b]Reference Re–H bond lengths in the isolated ReH_9^{2-} dianion calculated at the CCSD(T)/cc-pVQZ-PP level.[120] [c]Reference Re–H bond lengths reported in the neutron diffraction structure of K_2ReH_9.[121]

In summary, this example shows how the head-to-head comparison in bond strength of the same type of chemical bonding (even in the same fragment) can be conducted across different materials and the potential use of the local stretching frequencies as the root cause if red/blue-shift is observed in the measured vibrational frequencies among these materials.

4.2. Epoxy Bridge in Single Layered Graphite Oxide. In this example, we constructed a single-layered graphene oxide with one epoxy group being connected to a water molecule via a hydrogen bond (see Figure 4). This simplified
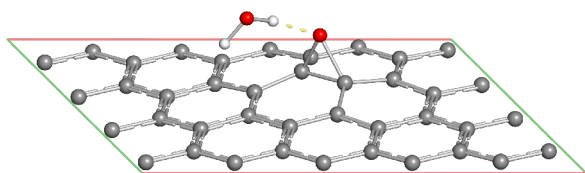

Figure 4. Primitive cell structure of a graphene oxide sheet with an epoxy bridge. A water molecule is attached to the bridging oxygen atom via hydrogen bonding.

model is conceptually adapted from the hydrated graphite oxide where the intermolecular hydrogen bonding network exists between water molecules and oxygen-containing functional groups.[124−126] In this model system, we are interested in the influence of the epoxy bridge as the defect on the CC bond strength in graphene as well as in the hydrogen bond strength between this epoxy group and the water molecule.

After cell optimization of this 5 × 4 primitive unit cell with the PBE density functional,[127] the graphene plane demonstrated partial nonplanarity centered around the epoxy bridge (see Figure 4 and Supporting Information Figure S2). This indicates the reduced delocalization of π electrons over the whole plane. After labeling the CC bonds in the graphene oxide into four different layers according to the distance (in terms of connectivity) toward the epoxy CC bond (see Figure 5), we calculated the local stretching force constants and frequencies of the CC bonds up to the fourth layer as listed in Table 4. In order to perform a straightforward comparison with the CC bonds in the commonly known chemical structures, we also calculated ethane, ethene, benzene, and graphene as the reference systems. We defined for this example a bond strength order function (BSO = $0.2820294 \cdot k^{0.8519586}$) which maps the local stretching force constants of the ethane single bond and ethene double bond to 1.0 and 2.0, respectively.[128] In this way, the local stretching force constants listed in Table 4 converted into the BSO scale can be more easily compared and interpreted.

First of all, the CC bond in the reference graphene layer is very close to the ethene double bond in terms of BSO. For the diatomic primitive cell structure of graphene, the local stretching vibrational mode corresponds to the degenerate modes around 1,600 cm^{-1}, and our calculated local stretching frequency matches well with the experimentally measured phonon frequencies at the Γ point (ca. 1,565 cm^{-1}).[129]
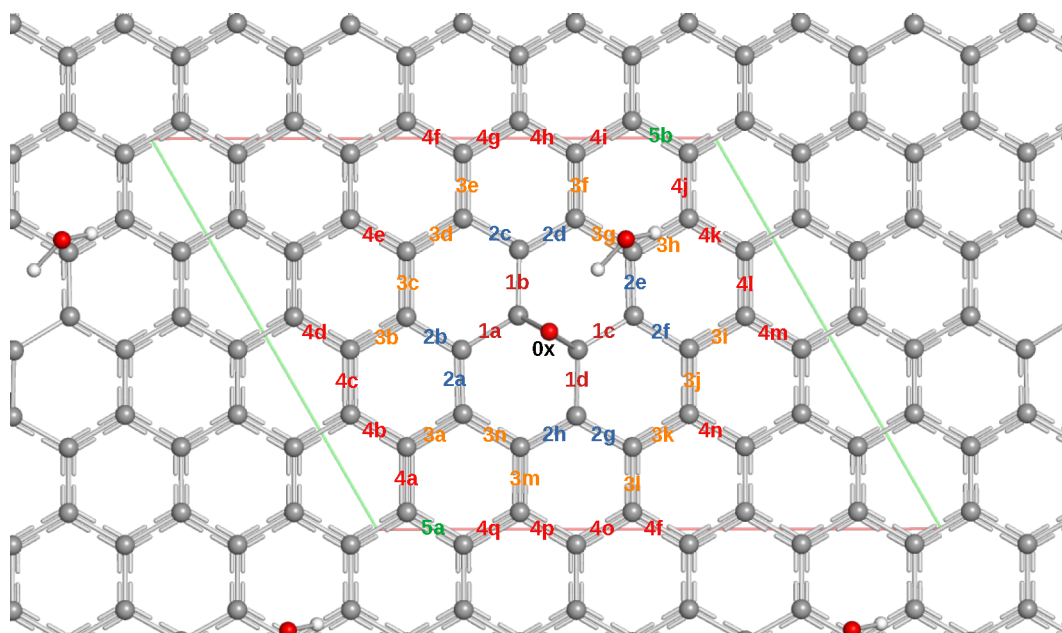
Figure 5. Top view of the two-dimensional graphene oxide model with labeled CC bonds in the 5 × 4 primitive unit cell. The epoxy bridge is positioned in the center of the primitive cell.

In this example system of graphene oxide, we found the strength of the studied CC bonds is equivalent to or lower than the benzene CC bond with BSO = 1.5. This is caused by the existence of the epoxy bridge which destroys the perfect π delocalization in the graphene layer. The epoxy CC bond is the weakest with BSO = 0.9, which is weaker than the single bond in the ethane molecule. Four CC bonds in the first layer have their BSO values increased to 1.2; and the CC bonds in the second layer are the strongest with BSO values equivalent to benzene, while their average local stretching force constant is larger than benzene by 0.1 mdyn/Å. For the third and fourth layers, their BSO values are 1.4, while the average local stretching force constant in the fourth layer is higher by 0.2 mdyn/Å.

We need to note that the calculated local stretching force constants of the CC bonds in this example system are expected to be dependent on the size of the primitive cell. In the current situation, we used a 5 × 4 unit cell with one epoxy group. For a larger unit cell having one epoxy group, one can expect that the CC bond strength would be closer to the graphene case because the space between two neighboring epoxy groups would be larger to accommodate the influence from the epoxy groups.

For the hydrogen bonding between water and the epoxy bridge in this example, we calculated its local stretching force constant and frequency. We used the water dimer and water−epoxide complex as the two reference systems with a single hydrogen bond (see Figure 6).

As listed in Table 5, the hydrogen bond and the donor O−H bond in the water dimer have their local stretching force constants as 0.189 and 7.005 mdyn/Å, respectively. When the acceptor molecule is changed into epoxide, the hydrogen bonding becomes slightly stronger (by 0.01 mdyn/Å), and the donor bond is weaker (by 0.4 mdyn/Å), which is consistent with the charge transfer picture of hydrogen bonding.[130] However, when the epoxide molecule is changed into the epoxy group in the graphene oxide, the hydrogen bond is substantially weakened by 0.13 mdyn/Å, and the O−H donor

bond is strengthened by 0.4 mdyn/Å. Two factors could be responsible for this difference including (1) the unique electronic structure of the epoxy bridge donating less lone pair electron density to water and (2) an antipush−antipull effect[131] caused by the existence of a second hydrogen bond between the water molecule and the π electron density of the graphene oxide layer (see Supporting Information Figure S3).[132]

In summary, this example shows how the strength of surface−adsorbate interaction can be quantified in terms of local stretching force constants which can act as a complement to the often used *adsorption energy*. In addition, the local stretching force constant can be used to detect the influence of the crystallographic defect on the strength of chemical bonds at different distances from the defect.

4.3. Microscopic Insight into Elastic Property of (DMA)[M(HCOO)₃] MOFs. Elasticity is a mechanical property of materials, and it describes the ability of a material to return to its original size and shape after an applied stress is removed.[133] Elasticity can be quantified with regard to different aspects including Young's modulus, bulk modulus, shear modulus, Poisson's ratio, and so forth. These elastic properties which can be experimentally measured or modeled by DFT calculations are macroscopic properties of materials; however, they are mainly determined by the chemical bonding between atoms at the microscopic level. Therefore, quantifying the chemical bond strength inside a material is expected to provide more detailed insight relevant to elastic properties.

In this example, a series of isostructural metal−organic frameworks (MOFs) named dimethylammonium (DMA) metal formate $[(CH_3)_2NH_2]M(HCOO)_3$ (M = divalent metal cation)[134] were selected to demonstrate the usefulness of local stretching force constants in understanding the elastic properties in terms of chemical bonding. In the work by Tan and co-workers,[135] the Young's moduli of four (DMA)[M-(HCOO)₃] MOF structures with different divalent metal cations (Mn^{2+}, Zn^{2+}, Co^{2+}, and Ni^{2+}) were measured experimentally, and they observed a linear correlation between

Table 4. Calculated Bond Lengths, Local Stretching Force Constants/Frequencies, and Bond Strength Orders of the CC Bonds in the Graphene Oxide Sheet and Reference Systems[a]

label	r	k_n^a	ω_n^a	BSO[b]	label	r	k_n^a	ω_n^a	BSO
0x	1.507	4.081	1074	0.9					
1a	1.470	5.677	1267	1.2	1d	1.470	5.702	1269	1.2
1b	1.470	5.690	1268	1.2	1c	1.471	5.668	1266	1.2
					average	1.470	5.684	1268	1.2
2a	1.411	6.993	1406	1.5	2h	1.411	7.006	1407	1.5
2d	1.411	7.020	1409	1.5	2e	1.412	6.964	1403	1.5
2b	1.414	6.932	1400	1.5	2g	1.413	6.963	1403	1.5
2c	1.412	6.973	1404	1.5	2f	1.414	6.932	1400	1.5
					average	1.412	6.973	1404	1.5
3a	1.430	6.557	1361	1.4	3m	1.430	6.555	1361	1.4
3f	1.430	6.562	1362	1.4	3h	1.430	6.562	1362	1.4
3b	1.428	6.668	1373	1.4	3l	1.428	6.667	1373	1.4
3e	1.427	6.668	1373	1.4	3i	1.429	6.655	1371	1.4
3c	1.436	6.428	1348	1.4	3k	1.437	6.419	1347	1.4
3d	1.436	6.430	1348	1.4	3j	1.435	6.439	1349	1.4
3n	1.449	6.153	1319	1.3	3g	1.450	6.137	1317	1.3
					average	1.434	6.493	1355	1.4
4a	1.430	6.601	1366	1.4	4i	1.431	6.577	1363	1.4
4q	1.431	6.582	1364	1.4	4j	1.431	6.574	1363	1.4
4b	1.427	6.686	1375	1.4	4p	1.426	6.718	1378	1.4
4h	1.426	6.730	1379	1.4	4k	1.428	6.663	1372	1.4
4c	1.427	6.701	1376	1.4	4o	1.426	6.741	1380	1.4
4g	1.426	6.741	1380	1.4	4l	1.427	6.689	1375	1.4
4d	1.427	6.720	1378	1.4	4f	1.426	6.721	1378	1.4
4m	1.427	6.723	1378	1.4	-				
4e	1.418	6.916	1398	1.5	4n	1.418	6.916	1398	1.5
					average	1.427	6.707	1377	1.4
5a	1.430	6.599	1366	1.4	5b	1.430	6.594	1365	1.4
					average	1.430	6.597	1366	1.4
refs									
ethane (C−C)	1.523	4.418	1117	1.0	ethene (C=C)	1.335	9.967	1678	2.0
benzene	1.399	6.844	1391	1.5	graphene	1.428	9.137	1607	1.9

[a]Units for bond length r, local stretching force constant k_n^a, and local stretching frequency ω_n^a are Å, mdyn/Å, and cm^{-1}, respectively. [b]The bond strength order for the CC bond is defined as the power function of the local stretching force constant with the ethane single bond and ethene double bond being 1.0 and 2.0, respectively (BSO = $0.2820294 \cdot k^{0.8519586}$).

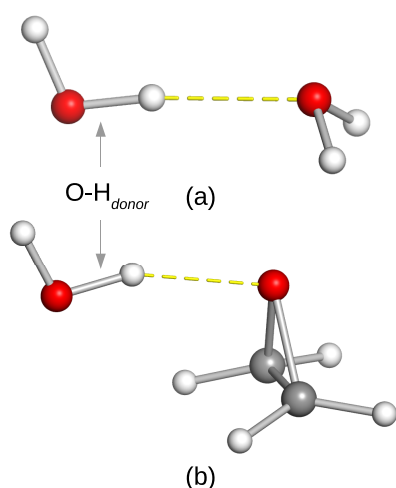**Figure 6.** Molecular structure of the (a) water dimer and (b) hydrogen-bonded adduct between water and epoxide.

Table 5. Calculated Bond Lengths, Local Stretching Force Constants, and Frequencies of the Hydrogen Bond and O−H Donor Bond in the Graphene Oxide Model and Two Molecular Reference Systems[a]

	H-bond			O−H donor		
	r	k_n^a	ω_n^a	r	k_n^a	ω_n^a
this example	2.019	0.074	364	0.981	7.052	3553
water dimer	1.887	0.189	582	0.983	7.005	3541
water + epoxide	1.835	0.205	606	0.987	6.593	3435

[a]Units for bond length r, local stretching force constant k_n^a, and local stretching frequency ω_n^a are Å, mdyn/Å, and cm^{-1}, respectively.

the Young's moduli and the ligand field stabilization energies of the four divalent cations in aquo complexes. In order to calculate the local stretching force constants of chemical bonds in these MOFs, we first optimized the primitive cell models of these MOF systems (see Figure 7) where the disordered dimethylammonium was treated as an ordered structure. By calculating the harmonic vibrational frequencies, we successfully obtained the local minimum structures for three MOFs where M = Zn^{2+}, Co^{2+}, and Ni^{2+}. However, the optimized MOF structure with Mn^{2+} led to a saddle-point structure with one imaginary frequency and was thus excluded from this work.
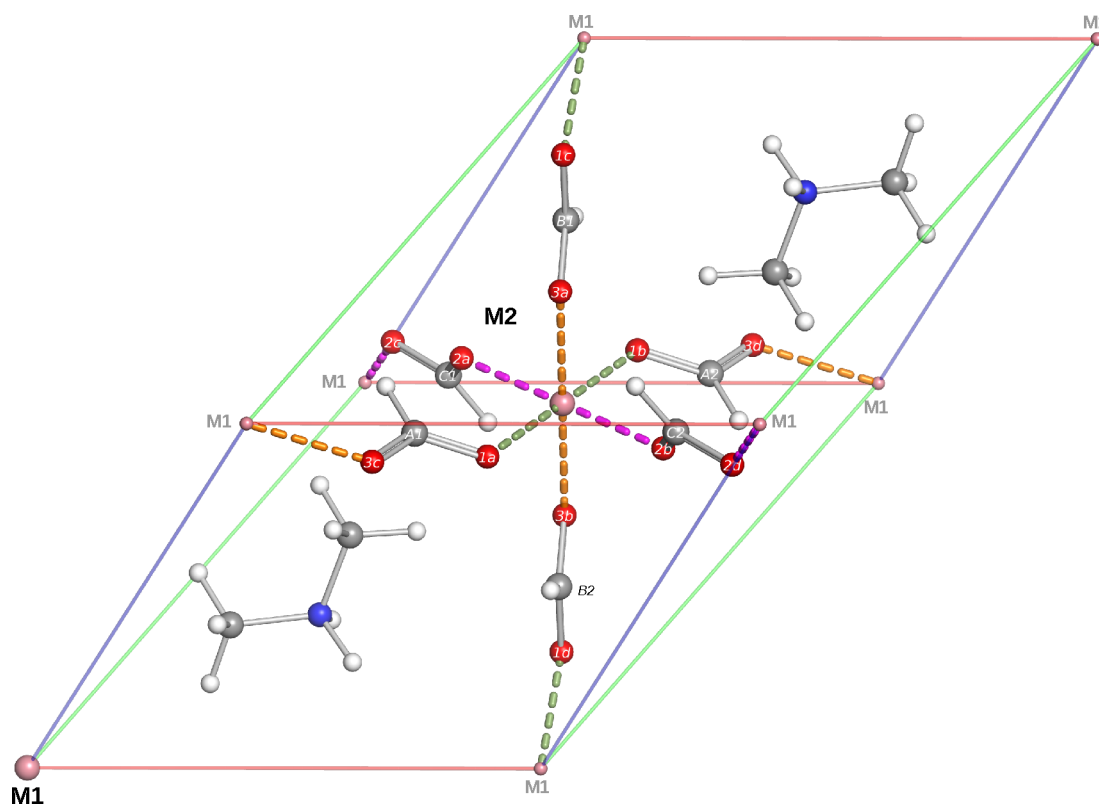
Figure 7. Primitive cell structure model of $(DMA)[M(HCOO)_3]$ metal−organic frameworks (M = Zn^{2+}, Co^{2+}, and Ni^{2+}). Each unit cell contains two metal atoms (M1 and M2), two dimethylammoniums, and six formate ligands. The metal−ligand bonds are shown with dashed lines, while the equivalent ones have the same color.

As shown in Figure 7, the $(DMA)[M(HCOO)_3]$ MOF structure is mainly supported by the metal−oxygen coordinate bonds and the formate C=O bonds, while the dimethylammoniums fill in the cavities.

At two equivalent MO_6 octahedral sites in the primitive cell model, there are three pairs of M−O bonds labeled with 1-M, 2-M, and 3-M. Each pair consists of two symmetry-equivalent M−O bonds (e.g., 1a-M2 and 1b-M2). In addition, we labeled the six formate carbon atoms as A, B, and C to facilitate the comparison of the C=O bonds. The local stretching force constants and frequencies for 12 M−O bonds and 12 C=O bonds in the primitive cell model of $(DMA)[M(HCOO)_3]$ MOF for three different metal cations are collected in Table 6.

The result shows that the local stretching force constants of 1-M and 2-M coordinate bonds are significantly larger than the 3-M type in all three MOFs. The average force constants of 1-M/2-M type coordinate bonds for Zn^{2+}, Co^{2+}, and Ni^{2+} are 0.63/0.75, 1.34/1.56, and 1.79/1.64 mdyn/Å, respectively. The 3-M coordinate bonds follow a reverse trend for these three MOFs to be 0.40, 0.35, and 0.14 mdyn/Å. The local stretching force constants of the formate C=O bonds in the MOF with Zn^{2+}, Co^{2+}, and Ni^{2+} are 7.8−8.5, 7.7−8.2, and 7.5−9.2 mdyn/Å, respectively. From the averaged M−O bond force constants for three MOFs, it seems that the ordering of force constants (0.591 < 1.083 < 1.189 mdyn/Å) is consistent with the ordering of the Young's moduli (19 < 22 < 24.5 GPa), but the averaged C=O bond force constants do not follow this trend.

An interesting point to note is that when we add the average M−O bond force constant to the average C=O bond force constant for each MOF structure, the sum is linearly correlated with the Young's moduli as shown in Figure 8. The underlying rationale justifying the summation of two average force constants is that there exists a 1:1 relationship between the M−O bond and C=O bond both supporting the MOF structures. This linear correlation between the local stretching force constants and Young's modulus partially reproduced the linear correlation between ligand field stabilization energy and Young's modulus for four MOFs,[135] while ours only involved three (excluding Mn^{2+}).

In summary, this example demonstrates how elastic properties can be dissected into the local stretching force constants of individual chemical bonds. In addition to elasticity, this approach can be potentially applied to other mechanical properties like hardness, strength and so forth to support the rational design of novel materials.

5. REMARKS ON LOCAL STRETCHING FORCE CONSTANT

5.1. Consistency in the Model Chemistry. As shown in this work and our previous publications, the local stretching force constant as a measure of bond strength is a powerful tool in comparing the same type of bond across different molecular/crystal structures, and it has strong relevance to the vibrational spectroscopy.[40] In the process of calculating local stretching force constants at the quantum chemical level, the model chemistry including density functional, integration grid, basis set, or/and pseudopotential should be consistent when describing different structures where the bond strengths are to be compared. Given the fact that different model chemistries lead to minor differences not only in the harmonic vibrational frequencies of the same structure but also in the

Table 6. Calculated Bond Lengths, Local Stretching Force Constants, and Frequencies of the Metal−Ligand Bonds and Formate CO Bonds in the (DMA)[M(HCOO)$_3$] MOF Structures (M = Zn^{2+}, Co^{2+}, and Ni^{2+})[a]

M−O	Zn^{2+} (19 GPa)[b]			Co^{2+} (22 GPa)[b]			Ni^{2+} (24.5 GPa)[b]		
	r	k_n^a	ω_n^a	r	k_n^a	ω_n^a	r	k_n^a	ω_n^a
1a-M2	2.091	0.623	287	1.920	1.336	424	1.866	1.778	490
1b-M2	2.091	0.630	288	1.920	1.332	424	1.866	1.792	492
1c-M1	2.091	0.628	288	1.919	1.341	425	1.866	1.773	489
1d-M1	2.091	0.631	289	1.919	1.338	425	1.866	1.799	493
2a-M2	2.067	0.747	314	1.916	1.560	459	1.887	1.659	473
2b-M2	2.067	0.747	314	1.916	1.559	459	1.887	1.640	471
2c-M1	2.067	0.749	314	1.916	1.562	459	1.887	1.643	471
2d-M1	2.067	0.750	315	1.916	1.562	459	1.887	1.620	468
3a-M2	2.171	0.394	228	2.186	0.349	217	2.819	0.140	138
3b-M2	2.171	0.398	229	2.186	0.350	217	2.821	0.133	134
3c-M1	2.171	0.397	229	2.189	0.351	218	2.822	0.149	142
3d-M1	2.171	0.399	229	2.189	0.352	218	2.823	0.136	136
average	2.110	0.591	277	2.008	1.083	367	2.191	1.189	366
C=O									
1a-A1	1.265	8.525	1452	1.275	8.196	1424	1.290	7.496	1362
1b-A2	1.265	8.536	1453	1.275	8.195	1424	1.290	7.480	1360
1c-B1	1.265	8.514	1451	1.275	8.198	1424	1.290	7.483	1361
1d-B2	1.265	8.537	1453	1.275	8.197	1424	1.290	7.487	1361
2a-C1	1.270	8.368	1439	1.276	8.199	1424	1.278	8.080	1414
2b-C2	1.270	8.334	1436	1.276	8.198	1424	1.278	8.038	1410
2c-C1	1.270	8.327	1435	1.276	8.198	1424	1.278	8.060	1412
2d-C2	1.270	8.371	1439	1.276	8.199	1424	1.278	8.051	1411
3a-B1	1.281	7.806	1390	1.280	7.741	1384	1.257	9.174	1507
3b-B2	1.281	7.813	1390	1.280	7.739	1384	1.257	9.186	1508
3c-A1	1.281	7.801	1389	1.279	7.755	1385	1.257	9.186	1508
3d-A2	1.281	7.816	1391	1.279	7.753	1385	1.257	9.161	1505
average	1.272	8.229	1427	1.277	8.047	1411	1.275	8.240	1427
sum of averages		8.820			9.130			9.429	

[a]Units for bond length r, local stretching force constant k_n^a, and local stretching frequency ω_n^a are Å, mdyn/Å, and cm^{-1}, respectively. [b]Experimentally measured Young's modulus E for corresponding MOF in the unit of GPa.
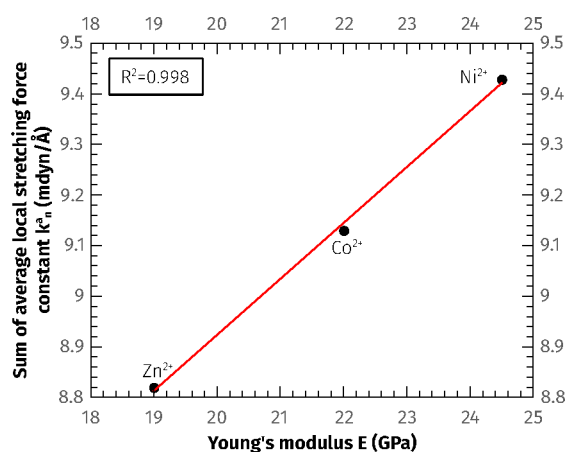

Figure 8. Sum of average local force constants of M−O and C=O bonds vs the Young's moduli for the (DMA)[M(HCOO)$_3$] MOF (M = Zn^{2+}, Co^{2+}, and Ni^{2+}).

local stretching force constant for the same bond in the same structure, the consistency in the level of theoretical calculation should be guaranteed to make the comparison of bond strengths legitimate.

However, if some inconsistency in the model chemistry is inevitable in calculating the local stretching force constants, the following three strategies can be applied to mitigate

discrepancies which cannot be completely eliminated. Supporting Information section S2 illustrates two of these strategies in detail.

5.1.1. Hessian Correction with Experimental Vibrational Frequencies. In the calculation of local stretching force constants, there are two factors which affect the accuracy of the result. The first is the harmonic approximation used when solving the vibrational problem, which overlooks the anharmonicity of the PES and the coupling of vibrational modes. The second is the performance of different levels of theory (e.g., density functionals) in calculating the Hessian matrix which leads to the experimentally measured fundamental frequencies. In the previous work,[128] we first calculated the vibrational mode vectors and corresponding frequencies and then replaced the calculated frequencies with the experimentally measured ones. In this way, a corrected Hessian matrix can be constructed for the local vibrational mode analysis. This approach eliminates the above two artifacts in calculating the local stretching force constants, but it only works for simple chemical systems like water molecule or diamond, because measuring and assigning the complete vibrational frequencies for slightly complex systems are in general challenging.

5.1.2. Empirical Scaling Factor. A different approach resembling the first strategy is to use the empirical scaling factors which are developed to match the calculated vibrational frequencies with the experimentally measured fundamental

frequencies (or the true harmonic frequencies).[136] If the scaling factor f is available for a given model chemistry, the square of this scaling factor f^2 can be multiplied with the calculated local stretching force constant according to eq 12. The major limitation of this approach is that there are only scaling factors for molecular systems but not for solids.

5.1.3. Bond Strength Order. In the previous work, we introduced and employed the bond strength order (BSO) as a function of the local stretching force constant in reminiscence of Pauling's bond order (BO).[128] The BSO can be defined as a power $(a \cdot k^b)$ or cubic function $(a \cdot k^3 + b \cdot k^2 + c \cdot k)$ of the local stretching force constant k_n^a, if two or three reference systems are selected, respectively.[137] With the BSO, we are able to put the local stretching force constants for the bonds of the same or different types into a unified scale for easy comparison. At the same time, the BSO method can help reduce the discrepancies of two different model chemistries applied in calculating local stretching force constants. For two different model chemistries X and Y, we can first select two or three reference systems and calculate the local stretching force constants at levels X and Y separately. As a result, either model chemistry has its own BSO definition. By mapping the local stretching force constants calculated at level X (or Y) into the BSO function defined at level X (or Y), we may compare the bond strength at the unified BSO scale. It is also possible to convert the local stretching force constants at level X into level Y via the X→BSO→Y path and vice versa.

5.2. Comparability of Local Stretching Force Constants. While using the local stretching force constant as a measure of bond strength, we often compare force constant values of the same type of bond A−B or the values between A−B and A−C where atoms B and C are in the same row/column in the periodic table. This is important because such comparison can provide chemical insights into the electronic factors influencing the bond strength. A prominent example in this regard is Badger's rule[138] and its generalization[139] which correlates the local stretching force constant and bond length for the same type of bond.

For two completely different bonds A−B and C−D, their local stretching force constants may not be useful for a direct comparison of bond strength; but from the physical rather than chemical point of view, their force constants interpreted as a measure of bond stiffness could be helpful in the analysis related to the mechanical properties.

6. CONCLUSIONS

In this manuscript, we have introduced LModeA-nano, a PyMOL plugin to carry out local vibrational mode analysis for periodic systems (including solids and surfaces) as well as isolated molecules to quantify the chemical bond strength in terms of local stretching force constants. The plugin is designed to be user-friendly and permits the selection of bond of interest for local vibrational mode analysis on the optimized chemical structure in a straightforward manner. The LModeA-nano code is freely available in GitHub, and it has been interfaced to various mainstream solid-state modeling packages as well as quantum chemistry packages.

7. COMPUTATIONAL DETAILS

The isolated ReH_9^{2-} dianion and K_2ReH_9 and Na_2ReH_9 solids (see section 4.1) were all described by the Gaussian and plane wave (GPW) approach[140] as implemented in the CP2K

package.[141] The revPBE functional[119] was chosen to model the molecule and solids paired with the short-range double-ζ DZVP-MOLOPT-SR-GTH basis set[142] and the GTH-PBE pseudopotential.[143,144] The planewave cutoff and the cutoff which controls the mapping of product Gaussians to the multigrid were set for the three systems to 750/70, 825/75, and 900/80 Ry, respectively, after delicate convergence testing. For the calculation of two solid systems, the Brillouin zone was sampled with a $5 \times 5 \times 8$ Monkhorst-Pack grid.[145] The geometry optimization of ReH_9^{2-} and the complete cell optimization of the primitive cell structures for two solids were considered converged when the maximum force component and maximum geometry change are below 0.000015 hartree/Bohr and 0.00006 Bohr, respectively. The vibrational frequencies and the Hessian matrix for the optimized ReH_9^{2-} structure were calculated numerically with analytic gradients using two displacements ($\Delta s = \pm 0.008$ Bohr) for each atom in X, Y, and Z directions. With the help of the Phonopy package,[62] the Hessian matrices for the primitive cells of K_2ReH_9 and Na_2ReH_9 were calculated in the same way with the displacement $\Delta s = \pm 0.005$ Å.

The two-dimensional graphene oxide system (see section 4.2) was described at the DFT level with the PBE functional[127] using the CRYSTAL17 package.[14] The pob-DZVP and 6-31+G(d,2p) basis sets were employed for elements C and O/H, respectively.[146−148] Grimme's empirical dispersion correction D3(BJ)[149] was added to the total energy and forces to better describe the interaction between water and graphene oxide. The shrinking factor of sampling points in the Pack-Monkhorst net was set to 20. The cell optimization of this 2D system was considered converged when the RMS deviation of gradient and displacement are below 0.000005 and 0.00001 au. The vibrational frequencies and Hessian matrix were calculated numerically with the displacement $\Delta s = \pm 0.003$ Å. The 2D graphene sheet as one reference system was calculated in a primitive cell model with the same level of theory except that the Grimme's D3(BJ) dispersion correction was not used. The reference molecules including ethane, ethene, benzene, water dimer, and the water−epoxide complex were calculated at the same level of theory as the graphene oxide model. In addition, a pruned XXLGRID (99,1454) integration grid[150] was employed for the DFT calculations with the CRYSTAL17 program.

Three $(DMA)[M(HCOO)_3]$ MOF structures (see section 4.3) were obtained by substituting the iron atoms in the $(DMA)[Fe(HCOO)_3]$ MOF with zinc, cobalt, or nickel atoms (M = Zn, Co, Ni). Then, the cell optimization of these three MOF structures was carried out at the GPW level with the CP2K package. The PBEsol density functional[151] was used to model these MOF systems along with the basis set and pseudopotential employed for the above-mentioned K_2ReH_9 solid. Grimme's D3(BJ) dispersion correction was also used. The planewave cutoff and the grid cutoff energies for these three MOF systems were set to 1100/75, 1100/70, 1100/75 Ry, respectively. The Brillouin zone was sampled with $6 \times 6 \times 6$, $10 \times 10 \times 10$, and $6 \times 6 \times 6$ Monkhorst-Pack grids, respectively, for the primitive cell models. The Hessian matrices of the optimized cell structures were calculated numerically with the help of Phonopy[62] as the K_2ReH_9 solid.

The input file templates for calculations with the CP2K package were generated using Multiwfn.[36] All figures for molecular and crystal structures in this work were prepared using our PyVibMS plugin[152] based on PyMOL.[106,107] All

calculations were conducted using the computational nodes equipped with dual Intel Xeon E5-2695 v4 CPUs (36 CPU cores) of the ManeFrame II supercomputers at SMU.

■ ASSOCIATED CONTENT

ⓈⒾ Supporting Information

The Supporting Information is available free of charge at https://pubs.acs.org/doi/10.1021/acs.jctc.1c01269.

> Additional figures, further discussion on consistency of model chemistry in calculating local stretching force constant, input file examples of CP2K and CRYSTAL17 programs, and Cartesian coordinates of showcase examples in this work (ZIP)

■ AUTHOR INFORMATION

Corresponding Authors

Yunwen Tao − *Department of Chemistry, Southern Methodist University, Dallas, Texas 75275-0314, United States*; Email: ywtao.smu@gmail.com

Elfi Kraka − *Department of Chemistry, Southern Methodist University, Dallas, Texas 75275-0314, United States*; ⓞ orcid.org/0000-0002-9658-5626; Email: ekraka@gmail.com

Authors

Wenli Zou − *Institute of Modern Physics, Northwest University, and Shaanxi Key Laboratory for Theoretical Physics Frontiers, Xi'an, Shaanxi 710127, P. R. China*; ⓞ orcid.org/0000-0002-0747-2428

Sadisha Nanayakkara − *Department of Chemistry, Southern Methodist University, Dallas, Texas 75275-0314, United States*

Complete contact information is available at:
https://pubs.acs.org/10.1021/acs.jctc.1c01269

Notes

The authors declare no competing financial interest.

■ ACKNOWLEDGMENTS

■ REFERENCES

(1) Pauling, L. *The Nature of the Chemical Bond and the Structure of Molecules and Crystals: An Introduction to Modern Structural Chemistry*; Cornell University Press: Ithaca, NY, 1960.

(2) Ruedenberg, K. Physical Nature of Chemical Bond. *Rev. Mod. Phys.* **1962**, *34*, 326−376.

(3) Maksic, Z. B., Ed. *Theoretical Models Of Chemical Bonding Part 2: The Concept Of The Chemical Bond*; Springer Verlag: Berlin, 1990.

(4) Frenking, G., Shaik, S., Eds. *The Chemical Bond: Chemical Bonding Across the Periodic Table*; Wiley-VCH: New York, 2014.

(5) Frenking, G., Shaik, S., Eds. *The Chemical Bond: Fundamental Aspects of Chemical Bonding*; Wiley-VCH: New York, 2014; DOI: 10.1002/9783527664696.

(6) Mingos, D., Ed. *The Chemical Bond, Vols. I—III − 100 Years Old and Getting Stronger*; Springer: Heidelberg, 2016.

(7) Frenking, G. The Chemical Bond − an Entrance Door of Chemistry to the Neighboring Sciences and to Philosophy. *Isr. J. Chem.* **2021**, DOI: 10.1002/ijch.202100070.

(8) Pauling, L. The Nature of the Chemical Bond. Application of Results Obtained from the Quantum Mechanics and from a Theory of Paramagnetic Susceptibility to the Structure of Molecules. *J. Am. Chem. Soc.* **1931**, *53*, 1367−1400.

(9) Becke, A. D.; Edgecombe, K. E. A Simple Measure of Electron Localization in Atomic and Molecular Systems. *J. Chem. Phys.* **1990**, *92*, 5397−5403.

(10) Giannozzi, P.; Baseggio, O.; Bonfà, P.; Brunato, D.; Car, R.; Carnimeo, I.; Cavazzoni, C.; de Gironcoli, S.; Delugas, P.; Ruffino, F. F.; Ferretti, A.; Marzari, N.; Timrov, I.; Urru, A.; Baroni, S. QuantumESPRESSO Toward the Exascale. *J. Chem. Phys.* **2020**, *152*, 154105.

(11) Johnson, E. R.; Keinan, S.; Mori-Sánchez, P.; Contreras-García, J.; Cohen, A. J.; Yang, W. Revealing Noncovalent Interactions. *J. Am. Chem. Soc.* **2010**, *132*, 6498−6506.

(12) Boto, R. A.; Contreras-García, J.; Tierny, J.; Piquemal, J.-P. *Interpretation of the Reduced Density Gradient* **2016**, *114*, 1406−1414.

(13) de Silva, P.; Corminboeuf, C. Simultaneous Visualization of Covalent and Noncovalent Interactions Using Regions of Density Overlap. *J. Chem. Theory Comput.* **2014**, *10*, 3745−3756.

(14) Dovesi, R.; Pascale, F.; Civalleri, B.; Doll, K.; Harrison, N. M.; Bush, I.; D'Arco, P.; Noël, Y.; Rérat, M.; Carbonnière, P.; Causà, M.; Salustro, S.; Lacivita, V.; Kirtman, B.; Ferrari, A. M.; Gentile, F. S.; Baima, J.; Ferrero, M.; Demichelis, R.; Pierre, M. D. L. The CRYSTAL Code, 1976−2020 and Beyond, A Long Story. *J. Chem. Phys.* **2020**, *152*, 204111.

(15) Bader, R. F. W. A Quantum Theory of Molecular Structure and its Applications. *Chem. Rev.* **1991**, *91*, 893−928.

(16) Bader, R. F. W. *Atoms in Molecules: A Quantum Theory*; Clarendon Press: Oxford, United Kingdom, 1994.

(17) Cremer, D.; Kraka, E. Chemical Bonds without Bonding Electron Density? Does the Difference Electron-Density Analysis Suffice for a Description of the Chemical Bond? *Angew. Chem., Int. Ed.* **1984**, *23*, 627−628.

(18) Hughbanks, T.; Hoffmann, R. Chains of Trans-Edge-Sharing Molybdenum Octahedra: Metal-Metal Bonding in Extended Systems. *J. Am. Chem. Soc.* **1983**, *105*, 3528−3537.

(19) Dronskowski, R.; Bloechl, P. E. Crystal Orbital Hamilton Populations (COHP): Energy-Resolved Visualization of Chemical Bonding in Solids Based on Density-Functional Calculations. *J. Phys. Chem.* **1993**, *97*, 8617−8624.

(20) Ruggiero, M. T.; Erba, A.; Orlando, R.; Korter, T. M. Origins of Contrasting Copper Coordination Geometries in Crystalline Copper Sulfate Pentahydrate. *Phys. Chem. Chem. Phys.* **2015**, *17*, 31023−31029.

(21) Raupach, M.; Tonner, R. A Periodic Energy Decomposition Analysis Method for the Investigation of Chemical Bonding in Extended Systems. *J. Chem. Phys.* **2015**, *142*, 194105.

(22) Zhao, L.; von Hopffgarten, M.; Andrada, D. M.; Frenking, G. Energy decomposition analysis. *WIREs Comput. Mol. Sci.* **2018**, *8*, e1345.

(23) Mao, Y.; Loipersberger, M.; Horn, P. R.; Das, A.; Demerdash, O.; Levine, D. S.; Veccham, S. P.; Head-Gordon, T.; Head-Gordon, M. From Intermolecular Interaction Energies and Observable Shifts to Component Contributions and Back Again: A Tale of Variational Energy Decomposition Analysis. *Annu. Rev. Phys. Chem.* **2021**, *72*, 641−666.

(24) Spackman, P. R.; Turner, M. J.; McKinnon, J. J.; Wolff, S. K.; Grimwood, D. J.; Jayatilaka, D.; Spackman, M. A. CrystalExplorer: A Program for Hirshfeld Surface Analysis, Visualization and Quantitative Analysis of Molecular Crystals. *J. Appl. Crystallogr.* **2021**, *54*, 1006−1011.
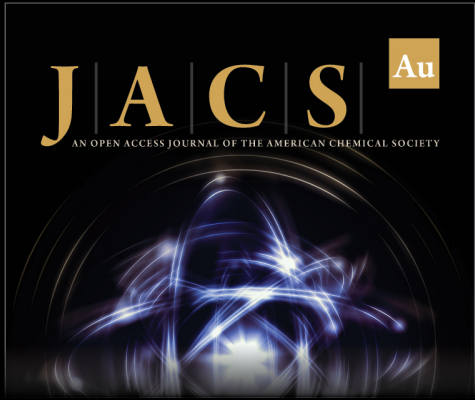
(25) Spackman, M. A.; Byrom, P. G. A Novel Definition of a Molecule in a Crystal. *Chem. Phys. Lett.* **1997**, *267*, 215−220.

(26) Spackman, M. A.; Jayatilaka, D. Hirshfeld Surface Analysis. *CrystEngComm* **2009**, *11*, 19−32.

(27) Nelson, R.; Ertural, C.; George, J.; Deringer, V. L.; Hautier, G.; Dronskowski, R. LOBSTER: Local Orbital Projections, Atomic Charges, and Chemical-Bonding Analysis from Projector-Augmented-Wave-Based Density-Functional Theory. *J. Comput. Chem.* **2020**, *41*, 1931−1940.

(28) Weinhold, F.; Landis, C.; Glendening, E. What Is NBO Analysis and How Is It Useful? *Int. Rev. Phys. Chem.* **2016**, *35*, 399−440.

(29) Landis, C. R.; Weinhold, F. *The Chemical Bond: Fundamental Aspects of Chemical Bonding*; John Wiley and Sons, Ltd.: 2014; Chapter 3, pp 91−120, DOI: 10.1002/9783527664696.ch3.

(30) Dunnington, B. D.; Schmidt, J. R. Generalization of Natural Bond Orbital Analysis to Periodic Systems: Applications to Solids and Surfaces via Plane-Wave Density Functional Theory. *J. Chem. Theory Comput.* **2012**, *8*, 1902−1911.

(31) Zubarev, D. Y.; Boldyrev, A. I. Developing Paradigms of Chemical Bonding: Adaptive Natural Density Partitioning. *Phys. Chem. Chem. Phys.* **2008**, *10*, 5207−5217.

(32) Galeev, T. R.; Dunnington, B. D.; Schmidt, J. R.; Boldyrev, A. I. Solid State Adaptive Natural Density Partitioning: A Tool for Deciphering Multi-Center Bonding in Periodic Systems. *Phys. Chem. Chem. Phys.* **2013**, *15*, 5022−5029.

(33) Otero-de-la-Roza, A.; Johnson, E. R.; Luaña, V. Critic2: A Program for Real-Space Analysis of Quantum Chemical Interactions in Solids. *Comput. Phys. Commun.* **2014**, *185*, 1007−1018.

(34) Vega, D.; Almeida, D. AIM-UC: An application for QTAIM analysis. *J. Comput. Methods Sci. Eng.* **2014**, *14*, 131−136.

(35) Kozlowski, D.; Pilmé, J. New Insights in Quantum Chemical Topology Studies Using Numerical Grid-Based Analyses. *J. Comput. Chem.* **2011**, *32*, 3207−3217.

(36) Lu, T.; Chen, F. Multiwfn: A Multifunctional Wavefunction Analyzer. *J. Comput. Chem.* **2012**, *33*, 580−592.

(37) Lefebvre, C.; Rubez, G.; Khartabil, H.; Boisson, J.-C.; Contreras-García, J.; Hénon, E. Accurately Extracting the Signature of Intermolecular Interactions Present in the NCI Plot of the Reduced Density Gradient versus Electron Density. *Phys. Chem. Chem. Phys.* **2017**, *19*, 17928−17936.

(38) Lu, T.; Chen, Q. Independent Gradient Model based on Hirshfeld Partition (IGMH): A New Method for Visual Study of Interactions in Chemical Systems. *ChemRxiv* **2021**, DOI: 10.26434/chemrxiv-2021-628vh.

(39) Lu, T.; Chen, Q. Interaction Region Indicator: A Simple Real Space Function Clearly Revealing Both Chemical Bonds and Weak Interactions. *Chem. Methods* **2021**, *1*, 231−239.

(40) Kraka, E.; Zou, W.; Tao, Y. Decoding Chemical Information from Vibrational Spectroscopy Data: Local Vibrational Mode Theory. *WIREs: Comput. Mol. Sci.* **2020**, *10*, e1480.

(41) Tao, Y.; Zou, W.; Sethio, D.; Verma, N.; Qiu, Y.; Tian, C.; Cremer, D.; Kraka, E. In Situ Measure of Intrinsic Bond Strength in Crystalline Structures: Local Vibrational Mode Theory for Periodic Systems. *J. Chem. Theory Comput.* **2019**, *15*, 1761−1776.

(42) Zhao, L.; Zhi, M.; Frenking, G. The Strength of a Chemical Bond. *Int. J. Quantum Chem.* **2021**, DOI: 10.1002/qua.26773.

(43) Jones, L. H. Infrared Spectra and Structure of the Crystalline Sodium Acetate Complexes of U(VI), Np(VI), Pu(VI), and Am(VI). A Comparison of Metal-Oxygen Bond Distance and Bond Force Constant in this Series. *J. Chem. Phys.* **1955**, *23*, 2105−2107.

(44) Lazarev, A. N.; Mirgorodsky, A. P. Molecular Force Constants in Dynamical Model of α-Quartz. *Phys. Chem. Miner.* **1991**, *18*, 231−243.

(45) Bagot, D.; Granger, R.; Rolland, S. A Comparison of Force Constants, Mechanical and Thermal Properties in $Hg_{1−x}Cd_xTe$ and $Hg_{1−x}Zn_xTe$ Mixed Crystals. *Phys. Stat. Sol. (b)* **1994**, *183*, 395−406.

(46) Postnikov, A. V.; Pagès, O.; Hugel, J. Lattice Dynamics of the Mixed Semiconductors (Be, Zn)Se from First-Principles Calculations. *Phys. Rev. B* **2005**, *71*, 115206.

(47) Sharma, P.; Rangra, V.; Sharma, P.; Katyal, S. Far-Infrared Study of Amorphous $Ge_{0.17}Se_{0.83−x}Sb_x$ Chalcogenide Glasses. *J. Alloys Compd.* **2009**, *480*, 934−937.

(48) Schnaars, D. D.; Wilson, R. E. Structural and Vibrational Properties of $U(VI)O_2Cl_4^{2−}$ and $Pu(VI)O_2Cl_4^{2−}$ Complexes. *Inorg. Chem.* **2013**, *52*, 14138−14147.

(49) de Groot, J.; Cassell, B.; Basile, M.; Fetrow, T.; Forbes, T. Z. Charge-Assisted Hydrogen-Bonding and Crystallization Effects within U^{VI} Glycine Compounds. *Eur. J. Inorg. Chem.* **2017**, *2017*, 1938−1946.

(50) Zordok, W.; Sadeek, S. A.; El-Farargy, A. F.; El-Lattif, N. S. A. Synthesis, Spectral, X-Ray Diffraction, DFT, and Nematicidal Activity of Mixed Ligand Complexes of Ethyl 2-(2-Hydroxybenzylidine)-Hydrazine Carboxylate and 1, 10-Phenanthroline with Some Transition Metals. *J. Chin. Chem. Soc.* **2017**, *64*, 1478−1495.

(51) Wang, H.; Hwang, J.; Zhang, C.; Wang, T.; Su, W.; Kim, H.; Kim, J.; Zhai, J.; Wang, X.; Park, H.; Kim, W.; Wang, C. Enhancement of the Thermoelectric Performance of Bulk SnTe Alloys via the Synergistic Effect of Band Structure Modification and Chemical Bond Softening. *J. Mater. Chem. A* **2017**, *5*, 14165−14173.

(52) El-Hamid, S. A.; El-Demerdash, R.; Arafat, H.; Sadeek, S. Spectroscopic Studies and Thermal Analysis of Mononuclear Metal Complexes with Moxifloxacin and 2, 2′-Bipyridine and Their Effects on Acute Lung Injury Induced by Hydrochloric Acid in Rats. *J. Mol. Struct.* **2017**, *1149*, 613−625.

(53) Nesbitt, H.; Henderson, G.; Bancroft, G.; O'Shaughnessy, C. Electron Densities over Si and O Atoms of Tetrahedra and Their Impact on Raman Stretching Frequencies and Si-NBO Force Constants. *Chem. Geol.* **2017**, *461*, 65−74.

(54) Aloui, T.; Fourati, N.; Guermazi, H.; Zerrouki, C.; Guermazi, S. Synthesis, Structural and Microstructural Study of New Fe-$Na_{0.5}H_{1.5}MoO_5$ Hybrid Material for Highly Efficient Energy Storage Hybrid Systems. *Inorg. Chem. Commun.* **2020**, *113*, 107811.

(55) Ateia, E. E.; Abdelmaksoud, M. K.; Ismail, H. A Study of the Magnetic Properties and the Magneto-Crystalline Anisotropy for the Nano-Composites $CoFe_2O_4/Sm_{0.7}La_{0.3}FeO_3$. *J. Mater. Sci.: Mater. Electron.* **2021**, *32*, 4480−4492.

(56) Lopes, L. B.; Vieira, L. H.; Assaf, J. M.; Assaf, E. M. Effect of Mg Substitution on $LaTi_{1−x}Mg_xO_{3+δ}$ Catalysts for Improving the C2 Selectivity of the Oxidative Coupling of Methane. *Catal. Sci. Technol.* **2021**, *11*, 283−296.

(57) Wilson, E. B.; Decius, J. C.; Cross, P. C. *Molecular Vibrations: The Theory of Infrared and Raman Vibrational Spectra*; Dover Publications: Mineola, NY, 2012.

(58) Sherwood, P. M. A. *Vibrational Spectroscopy of Solids*; Cambridge University Press: Cambridge, 2011.

(59) Tadaaki, N.; Kazuo, K.; Yoshitaka, I.; Chuhei, O.; Otani, S. Surface Phonons of $LaB_6(100)$: Deformation of Boron Octahedra at the Surface. *Surf. Sci.* **1993**, *290*, 436−444.

(60) Gupta, H.; Singh, M. K.; Tiwari, L. Zone Center Frequencies of Tetragonal $CdAl_2Se_4$. *J. Solid State Chem.* **2000**, *153*, 317−320.

(61) Aizawa, T.; Hayami, W.; Otani, S. Surface Phonon Dispersion of $ZrB_2(0001)$ and $NbB_2(0001)$. *Phys. Rev. B* **2001**, *65*, 024303.

(62) Togo, A.; Tanaka, I. First Principles Phonon Calculations in Materials Science. *Scr. Mater.* **2015**, *108*, 1−5.

(63) Kumar, V. Interatomic Force Constants of Semiconductors. *J. Phys. Chem. Solids* **2000**, *61*, 91−94.

(64) Brown, I. D.; Klages, P.; Skowron, A. Influence of Pressure on the Lengths of Chemical Bonds. *Acta Cryst. B* **2003**, *59*, 439−448.

(65) Verma, A. Bond-Stretching and Bond-Bending Force Constant of Binary Tetrahedral ($A^{III}B^V$ and $A^{II}B^{VI}$) Semiconductors. *Phys. Lett. A* **2008**, *372*, 7196−7198.

(66) Verma, A. Bond-Stretching Force Constant of $A^IB^{III}C_2^{VI}$ and $A^{II}B^{IV}C_2^V$ Chalcopyrite Semiconductors. *Solid State Commun.* **2009**, *149*, 1236−1239.

(67) Batsanov, S. S. System of Metal Electronegativities Calculated from the Force Constants of the Bonds. *Russ. J. Inorg. Chem.* **2011**, *56*, 906−912.

(68) Kaya, S.; Chamorro, E.; Petrov, D.; Kaya, C. New Insights from the Relation between Lattice Energy and Bond Stretching Force Constant in Simple Ionic Compounds. *Polyhedron* **2017**, *123*, 411−418.

(69) Batsanov, S. S.; Batsanov, A. S. Solid-State Electronegativity of Atoms: New Approaches. *Acta Cryst. B* **2021**, *77*, 495−505.

(70) Ren, L.; Wang, H.; Tu, B.; Xu, P.; Zong, X.; Wang, W.; Fu, Z. Investigation on composition-dependent properties of $Mg_{5x}Al_{23-5x}O_{27+5x}N_{5-5x}$ ($0 \leq x \leq 1$): Part II. Mechanical Properties via First-Principles Calculations Combined with Bond Valence Models. *J. Eur. Ceram. Soc.* **2021**, *41*, 4942−4950.

(71) Joghlaf, M.; Ababou, Y.; Sayouri, S. A Simple Approach to Compute Interatomic Force Constant for Mono and Diatomic Semiconductors. *J. Appl. Math. Phys.* **2021**, *09*, 11−20.

(72) Aniya, M. Interatomic Force Constants and Localized Effective Charges in Copper Halides. *Solid State Ion.* **1999**, *121*, 281−284.

(73) Tanaka, K.; Inui, H.; Yamaguchi, M.; Koiwa, M. Directional Atomic Bonds in $MoSi_2$ and Other Transition-Metal Disilicides with the $C11_b$, C40 and C54 structures. *Mater. Sci. Eng., A* **1999**, *261*, 158−164.

(74) El-Mallawany, R. Structural Interpretations on Tellurite Glasses. *Mater. Chem. Phys.* **2000**, *63*, 109−115.

(75) Dolocan, V.; Dolocan, A.; Dolocan, V. O. Relation of Inter-Atomic Forces in Solids to Bulk Modulus, Cohesive Energy and Thermal Expansion. *Mod. Phys. Lett. B* **2008**, *22*, 2481−2492.

(76) Genoese, A.; Genoese, A.; Rizzi, N. L.; Salerno, G. Force Constants of BN, SiC, AlN and GaN Sheets Through Discrete Homogenization. *Meccanica* **2018**, *53*, 593−611.

(77) Alam, M.; Shah, M.; Nuruzzaman, M.; Hadi, M.; Parvin, F.; Zilani, M. Effect of Hydrostatic Compression on Physical Properties of Li_2TmSi_3 (Tm = Ir, Pt, Rh, Os) with Ground-State Optical Features. *J. Phys. Chem. Solids* **2021**, *156*, 110124.

(78) Dauphas, N.; Roskosz, M.; Alp, E.; Golden, D.; Sio, C.; Tissot, F.; Hu, M.; Zhao, J.; Gao, L.; Morris, R. A General Moment NRIXS Approach to the Determination of Equilibrium Fe Isotopic Fractionation Factors: Application to Goethite and Jarosite. *Geochim. Cosmochim. Acta* **2012**, *94*, 254−275.

(79) Zeng, H.; Rozsa, V. F.; Nie, N. X.; Zhang, Z.; Pham, T. A.; Galli, G.; Dauphas, N. Ab Initio Calculation of Equilibrium Isotopic Fractionations of Potassium and Rubidium in Minerals and Water. *ACS Earth Space Chem.* **2019**, *3*, 2601−2612.

(80) Wang, W.; Huang, S.; Huang, F.; Zhao, X.; Wu, Z. Equilibrium Inter-Mineral Titanium Isotope Fractionation: Implication for High-Temperature Titanium Isotope Geochemistry. *Geochim. Cosmochim. Acta* **2020**, *269*, 540−553.

(81) Aarons, S. M.; Dauphas, N.; Blanchard, M.; Zeng, H.; Nie, N. X.; Johnson, A. C.; Greber, N. D.; Hopp, T. Clues from Ab Initio Calculations on Titanium Isotopic Fractionation in Tholeiitic and Calc-Alkaline Magma Series. *ACS Earth Space Chem.* **2021**, *5*, 2466−2480.

(82) Lee, C.; Gonze, X. Lattice Dynamics and Dielectric Properties of SiO_2 Stishovite. *Phys. Rev. Lett.* **1994**, *72*, 1686−1689.

(83) Shang, S.-L.; Hector, L. G.; Shi, S.; Qi, Y.; Wang, Y.; Liu, Z.-K. Lattice Dynamics, Thermodynamics and Elastic Properties of monoclinic Li_2CO_3 from Density Functional Theory. *Acta Mater.* **2012**, *60*, 5204−5216.

(84) Deringer, V. L.; Stoffel, R. P.; Wuttig, M.; Dronskowski, R. Vibrational Properties and Bonding Nature of Sb_2Se_3 and Their Implications for Chalcogenide Materials. *Chem. Sci.* **2015**, *6*, 5255−5262.

(85) Shang, S.-L.; Wang, Y.; Gleeson, B.; Liu, Z.-K. Understanding Slow-Growing Alumina Scale Mediated by Reactive Elements: Perspective via Local Metal-Oxygen Bonding Strength. *Scr. Mater.* **2018**, *150*, 139−142.

(86) Vila, F. D.; Hayashi, S. T.; Rehr, J. J. Efficient Calculation of the Negative Thermal Expansion in ZrW_2O_8. *Front. Chem.* **2018**, *6*, 296.

(87) Yue, S.-Y.; Xu, T.; Liao, B. Ultralow Thermal Conductivity in a Two-Dimensional Material due to Surface-Enhanced Eesonant Bonding. *Mater. Today Phys.* **2018**, *7*, 89−95.

(88) Khazaei, M.; Ranjbar, A.; Esfarjani, K.; Bogdanovski, D.; Dronskowski, R.; Yunoki, S. Insights into Exfoliation Possibility of MAX Phases to MXenes. *Phys. Chem. Chem. Phys.* **2018**, *20*, 8579−8592.

(89) Khazaei, M.; Wang, J.; Estili, M.; Ranjbar, A.; Suehara, S.; Arai, M.; Esfarjani, K.; Yunoki, S. Novel MAB Phases and Insights into Their Exfoliation into 2D MBenes. *Nanoscale* **2019**, *11*, 11305−11314.

(90) Manzoor, A.; Aidhy, D. S. Predicting Vibrational Entropy of fcc Solids Uniquely from Bond Chemistry Using Machine Learning. *Materialia* **2020**, *12*, 100804.

(91) Hempelmann, J.; Müller, P. C.; Konze, P. M.; Stoffel, R. P.; Steinberg, S.; Dronskowski, R. Long-Range Forces in Rock-Salt-Type Tellurides and How they Mirror the Underlying Chemical Bonding. *Adv. Mater.* **2021**, *33*, 2100163.

(92) Chong, X.; Palma, J. P. S.; Wang, Y.; Shang, S.-L.; Drymiotis, F.; Ravi, V. A.; Star, K. E.; Fleurial, J.-P.; Liu, Z.-K. Thermodynamic Properties of the Yb-Sb System Predicted from First-Principles Calculations. *Acta Mater.* **2021**, *217*, 117169.

(93) Yanagisawa, H.; Tanaka, T.; Ishida, Y.; Rokuta, E.; Otani, S.; Oshima, C. Phonon Dispersion Curves of Stable and Metastable BC_3 Honeycomb Epitaxial Sheets and Their Chemical Bonding: Experiment and Theory. *Phys. Rev, B* **2006**, *73*, 045412.

(94) Tapia, A.; Cab, C.; Hernández-Pérez, A.; Villanueva, C.; Peñuñuri, F.; Avilés, F. The Bond Force Constants and Elastic Properties of Boron Nitride Nanosheets and Nanoribbons Using a Hierarchical Modeling Approach. *Physica E* **2017**, *89*, 183−193.

(95) Grzyb, T.; Szczeszak, A.; Shyichuk, A.; Moura, R. T.; Neto, A. N. C.; Andrzejewska, N.; Malta, O. L.; Lis, S. Comparative Studies of Structure, Spectroscopic Properties and Intensity Parameters of Tetragonal Rare Earth Vanadate Nanophosphors Doped with Eu(III). *J. Alloys Compd.* **2018**, *741*, 459−472.

(96) Jones, L. H.; Swanson, B. I. Interpretation of Potential Constants: Application to Study of Bonding Forces in Metal Cyanide Complexes and Metal Carbonyls. *Acc. Chem. Res.* **1976**, *9*, 128−134.

(97) Grunenberg, J. Ill-Defined Concepts in Chemistry: Rigid Force Constants vs. Compliance Constants as Bond Strength Descriptors for the Triple Bond in Diboryne. *Chem. Sci.* **2015**, *6*, 4086−4088.

(98) Zou, W.; Tao, Y.; Freindorf, M.; Cremer, D.; Kraka, E. Local Vibrational Force Constants - From the Assessment of Empirical Force Constants to the Description of Bonding in Large Systems. *Chem. Phys. Lett.* **2020**, *748*, 137337.

(99) Konkoli, Z.; Cremer, D. A New Way of Analyzing Vibrational Spectra. I. Derivation of Adiabatic Internal Modes. *Int. J. Quantum Chem.* **1998**, *67*, 1−9.

(100) Konkoli, Z.; Larsson, J. A.; Cremer, D. A New Way of Analyzing Vibrational Spectra. II. Comparison of Internal Mode Frequencies. *Int. J. Quantum Chem.* **1998**, *67*, 11−27.

(101) Konkoli, Z.; Cremer, D. A New Way of Analyzing Vibrational Spectra. III. Characterization of Normal Vibrational Modes in terms of Internal Vibrational Modes. *Int. J. Quantum Chem.* **1998**, *67*, 29−40.

(102) Konkoli, Z.; Larsson, J. A.; Cremer, D. A New Way of Analyzing Vibrational Spectra. IV. Application and Testing of Adiabatic Modes within the Concept of the Characterization of Normal Modes. *Int. J. Quantum Chem.* **1998**, *67*, 41−55.

(103) Zou, W.; Kalescky, R.; Kraka, E.; Cremer, D. Relating Normal Vibrational Modes to Local Vibrational Modes with the Help of an Adiabatic Connection Scheme. *J. Chem. Phys.* **2012**, *137*, 084114.

(104) Wilson, E. B. A Method of Obtaining the Expanded Secular Equation for the Vibration Frequencies of A Molecule. *J. Chem. Phys.* **1939**, *7*, 1047−1052.

(105) Kalescky, R.; Zou, W.; Kraka, E.; Cremer, D. Local Vibrational Modes of the Water Dimer - Comparison of Theory and Experiment. *Chem. Phys. Lett.* **2012**, *554*, 243−247.

(106) DeLano, W. L. *The PyMOL Molecular Graphics System*; DeLano Scientific: San Carlos, CA, USA, 2002.

(107) Schrödinger, LLC., *The PyMOL Molecular Graphics System*, Version 2.0; 2017.

(108) Chaput, L.; Togo, A.; Tanaka, I.; Hug, G. Phonon-Phonon Interactions in Transition Metals. *Phys. Rev. B* **2011**, *84*, 094302.

(109) Parlinski, K.; Li, Z. Q.; Kawazoe, Y. First-Principles Determination of the Soft Mode in Cubic ZrO₂. *Phys. Rev. Lett.* **1997**, *78*, 4063−4066.

(110) Yang, T.; Berry, J. F. Numerical Nuclear Second Derivatives on a Computing Grid: Enabling and Accelerating Frequency Calculations on Complex Molecular Systems. *J. Chem. Theory Comput.* **2018**, *14*, 3459−3467.

(111) Frisch, M. J.; Trucks, G. W.; Schlegel, H. B.; Scuseria, G. E.; Robb, M. A.; Cheeseman, J. R.; Scalmani, G.; Barone, V.; Petersson, G. A.; Nakatsuji, H.; Li, X.; Caricato, M.; Marenich, A. V.; Bloino, J.; Janesko, B. G.; Gomperts, R.; Mennucci, B.; Hratchian, H. P.; Ortiz, J. V.; Izmaylov, A. F.; Sonnenberg, J. L.; Williams-Young, D.; Ding, F.; Lipparini, F.; Egidi, F.; Goings, J.; Peng, B.; Petrone, A.; Henderson, T.; Ranasinghe, D.; Zakrzewski, V. G.; Gao, J.; Rega, N.; Zheng, G.; Liang, W.; Hada, M.; Ehara, M.; Toyota, K.; Fukuda, R.; Hasegawa, J.; Ishida, M.; Nakajima, T.; Honda, Y.; Kitao, O.; Nakai, H.; Vreven, T.; Throssell, K.; Montgomery, J. A., Jr.; Peralta, J. E.; Ogliaro, F.; Bearpark, M. J.; Heyd, J. J.; Brothers, E. N.; Kudin, K. N.; Staroverov, V. N.; Keith, T. A.; Kobayashi, R; Normand, J.; Raghavachari, K.; Rendell, A. P.; Burant, J. C.; Iyengar, S. S.; Tomasi, J.; Cossi, M.; Millam, J. M.; Klene, M.; Adamo, C.; Cammi, R.; Ochterski, J. W.; Martin, R. L.; Morokuma, K.; Farkas, O.; Foresman, J. B.; Fox, D. J. *Gaussian 16*, Revision B.01; Gaussian Inc.: Wallingford, CT, 2016.

(112) Epifanovsky, E.; Gilbert, A. T. B.; Feng, X.; Lee, J.; Mao, Y.; Mardirossian, N.; Pokhilko, P.; White, A. F.; Coons, M. P.; Dempwolff, A. L.; Gan, Z.; Hait, D.; Horn, P. R.; Jacobson, L. D.; Kaliman, I.; Kussmann, J.; Lange, A. W.; Lao, K. U.; Levine, D. S.; Liu, J.; McKenzie, S. C.; Morrison, A. F.; Nanda, K. D.; Plasser, F.; Rehn, D. R.; Vidal, M. L.; You, Z.-Q.; Zhu, Y.; Alam, B.; Albrecht, B. J.; Aldossary, A.; Alguire, E.; Andersen, J. H.; Athavale, V.; Barton, D.; Begam, K.; Behn, A.; Bellonzi, N.; Bernard, Y. A.; Berquist, E. J.; Burton, H. G. A.; Carreras, A.; Carter-Fenk, K.; Chakraborty, R.; Chien, A. D.; Closser, K. D.; Cofer-Shabica, V.; Dasgupta, S.; de Wergifosse, M.; Deng, J.; Diedenhofen, M.; Do, H.; Ehlert, S.; Fang, P.-T.; Fatehi, S.; Feng, Q.; Friedhoff, T.; Gayvert, J.; Ge, Q.; Gidofalvi, G.; Goldey, M.; Gomes, J.; González-Espinoza, C. E.; Gulania, S.; Gunina, A. O.; Hanson-Heine, M. W. D.; Harbach, P. H. P.; Hauser, A.; Herbst, M. F.; Hernández Vera, M.; Hodecker, M.; Holden, Z. C.; Houck, S.; Huang, X.; Hui, K.; Huynh, B. C.; Ivanov, M.; Jász, A.; Ji, H.; Jiang, H.; Kaduk, B.; Kähler, S.; Khistyaev, K.; Kim, J.; Kis, G.; Klunzinger, P.; Koczor-Benda, Z.; Koh, J. H.; Kosenkov, D.; Koulias, L.; Kowalczyk, T.; Krauter, C. M.; Kue, K.; Kunitsa, A.; Kus, T.; Ladjánszki, I.; Landau, A.; Lawler, K. V.; Lefrancois, D.; Lehtola, S.; Li, R. R.; Li, Y.-P.; Liang, J.; Liebenthal, M.; Lin, H.-H.; Lin, Y.-S.; Liu, F.; Liu, K.-Y.; Loipersberger, M.; Luenser, A.; Manjanath, A.; Manohar, P.; Mansoor, E.; Manzer, S. F.; Mao, S.-P.; Marenich, A. V.; Markovich, T.; Mason, S.; Maurer, S. A.; McLaughlin, P. F.; Menger, M. F. S. J.; Mewes, J.-M.; Mewes, S. A.; Morgante, P.; Mullinax, J. W.; Oosterbaan, K. J.; Paran, G.; Paul, A. C.; Paul, S. K.; Pavošević, F.; Pei, Z.; Prager, S.; Proynov, E. I.; Rák, Á.; Ramos-Cordoba, E.; Rana, B.; Rask, A. E.; Rettig, A.; Richard, R. M.; Rob, F.; Rossomme, E.; Scheele, T.; Scheurer, M.; Schneider, M.; Sergueev, N.; Sharada, S. M.; Skomorowski, W.; Small, D. W.; Stein, C. J.; Su, Y.-C.; Sundstrom, E. J.; Tao, Z.; Thirman, J.; Tornai, G. J.; Tsuchimochi, T.; Tubman, N. M.; Veccham, S. P.; Vydrov, O.; Wenzel, J.; Witte, J.; Yamada, A.; Yao, K.; Yeganeh, S.; Yost, S. R.; Zech, A.; Zhang, I. Y.; Zhang, X.; Zhang, Y.; Zuev, D.; Aspuru-Guzik, A.; Bell, A. T.; Besley, N. A.; Bravaya, K. B.; Brooks, B. R.; Casanova, D.; Chai, J.-D.; Coriani, S.; Cramer, C. J.; Cserey, G.; DePrince, A. E.; DiStasio, R. A.; Dreuw, A.; Dunietz, B. D.; Furlani, T. R.; Goddard, W. A.; Hammes-Schiffer, S.; Head-Gordon, T.; Hehre, W. J.; Hsu, C.-P.; Jagau, T.-C.; Jung, Y.; Klamt, A.; Kong, J.; Lambrecht, D. S.; Liang, W.; Mayhall, N. J.; McCurdy, C. W.; Neaton, J. B.; Ochsenfeld, C.; Parkhill, J. A.; Peverati, R.; Rassolov, V. A.; Shao, Y.; Slipchenko, L. V.; Stauch, T.; Steele, R. P.; Subotnik, J. E.; Thom, A. J. W.; Tkatchenko, A.; Truhlar, D. G.; Van Voorhis, T.; Wesolowski, T. A.; Whaley, K. B.; Woodcock, H. L.; Zimmerman, P. M.; Faraji, S.; Gill,

P. M. W.; Head-Gordon, M.; Herbert, J. M.; Krylov, A. I. Software for the Frontiers of Quantum Chemistry: An Overview of Developments in the Q-Chem 5 Package. *J. Chem. Phys.* **2021**, *155*, 084801.

(113) Zou, W.; Tao, Y. UniMoVib: A Unified Interface for Molecular Harmonic Vibrational Frequency Calculations. 2020. https://github.com/zorkzou/UniMoVib (accessed 2022-02-11).

(114) Tao, Y.; Qiu, Y.; Zou, W.; Nanayakkara, S.; Yannacone, S.; Kraka, E. In Situ Assessment of Intrinsic Strength of X-I···OA Type Halogen Bonds in Molecular Crystals with Periodic Local Vibrational Mode Theory. *Molecules* **2020**, *25*, 1589.

(115) Nanayakkara, S.; Tao, Y.; Kraka, E. Capturing Individual Hydrogen Bond Strengths in Ices via Periodic Local Vibrational Mode Theory: Beyond the Lattice Energy Picture. *J. Chem. Theory Comput.* **2022**, *18*, 562−579.

(116) King, R. Structure and Bonding in Homoleptic Transition Metal Hydride Anions. *Coord. Chem. Rev.* **2000**, *200−202*, 813−829.

(117) Knox, K.; Ginsberg, A. P. X-Ray Determination of the Crystal Structure of Potassium Rhenium Hydride. *Inorg. Chem.* **1964**, *3*, 555−558.

(118) Abrahams, S. C.; Ginsberg, A. P.; Knox, K. Transition Metal-Hydrogen Compounds. II. The Crystal and Molecular Structure of Potassium Rhenium Hydride, K₂ReH₉. *Inorg. Chem.* **1964**, *3*, 558−567.

(119) Zhang, Y.; Yang, W. Comment on "Generalized Gradient Approximation Made Simple. *Phys. Rev. Lett.* **1998**, *80*, 890−890.

(120) Li, C.; Agarwal, J.; Schaefer, H. F. The Remarkable [ReH₉]²⁻ Dianion: Molecular Structure and Vibrational Frequencies. *J. Phys. Chem. B* **2014**, *118*, 6482−6490.

(121) Bronger, W.; à Brassard, L.; Müller, P.; Lebech, B.; Schultz, T. K₂ReH₉, eine Neubestimmung der Struktur. *Z. Anorg. Allg. Chem.* **1999**, *625*, 1143−1146.

(122) Pauling, L. The Nature of the Chemical Bond. IV. The Energy of Single Bonds and the Relative Electronegativity of Atoms. *J. Am. Chem. Soc.* **1932**, *54*, 3570−3582.

(123) Fried, S. D.; Boxer, S. G. Measuring Electric Fields and Noncovalent Interactions Using the Vibrational Stark Effect. *Acc. Chem. Res.* **2015**, *48*, 998−1006.

(124) He, H.; Klinowski, J.; Forster, M.; Lerf, A. A New Structural Model for Graphite Oxide. *Chem. Phys. Lett.* **1998**, *287*, 53−56.

(125) Dreyer, D. R.; Park, S.; Bielawski, C. W.; Ruoff, R. S. The Chemistry of Graphene Oxide. *Chem. Soc. Rev.* **2010**, *39*, 228−240.

(126) Liu, L.; Zhang, R.; Liu, Y.; Tan, W.; Zhu, G. Insight into Hydrogen Bonds and Characterization of Interlayer Spacing of Hydrated Graphene Oxide. *J. Mol. Model.* **2018**, *24*, 137.

(127) Perdew, J. P.; Burke, K.; Ernzerhof, M. Generalized Gradient Approximation Made Simple. *Phys. Rev. Lett.* **1996**, *77*, 3865−3868.

(128) Zou, W.; Cremer, D. C₂ in a Box: Determining its Intrinsic Bond Strength for the $X^1\Sigma_g^+$ Ground State. *Chem.—Eur. J.* **2016**, *22*, 4087−4097.

(129) Maultzsch, J.; Reich, S.; Thomsen, C.; Requardt, H.; Ordejón, P. Phonon Dispersion in Graphite. *Phys. Rev. Lett.* **2004**, *92*, 075501.

(130) Weinhold, F.; Glendening, E. D. Comment on "Natural Bond Orbitals and the Nature of the Hydrogen Bond. *J. Phys. Chem. A* **2018**, *122*, 724−732.

(131) Tao, Y.; Zou, W.; Kraka, E. Strengthening of Hydrogen Bonding With the Push-Pull Effect. *Chem. Phys. Lett.* **2017**, *685*, 251−258.

(132) Nekoei, A.-R.; Vatanparast, M. π-Hydrogen Bonding and Aromaticity: A Systematic Interplay Study. *Phys. Chem. Chem. Phys.* **2019**, *21*, 623−630.

(133) Sadd, M. *Elasticity: Theory, Applications, and Numerics*; Elsevier/Academic Press: Amsterdam, Boston, 2009; DOI: 10.1016/B978-0-12-374446-3.X0001-6.

(134) Jain, P.; Ramachandran, V.; Clark, R. J.; Zhou, H. D.; Toby, B. H.; Dalal, N. S.; Kroto, H. W.; Cheetham, A. K. Multiferroic Behavior Associated with an Order-Disorder Hydrogen Bonding Transition in Metal-Organic Frameworks (MOFs) with the Perovskite ABX₃ Architecture. *J. Am. Chem. Soc.* **2009**, *131*, 13625−13627.

(135) Tan, J.-C.; Jain, P.; Cheetham, A. K. Influence of Ligand Field Stabilization Energy on the Elastic Properties of Multiferroic MOFs with the Perovskite Architecture. *Dalton Trans.* **2012**, *41*, 3949−3952.

(136) Alecu, I. M.; Zheng, J.; Zhao, Y.; Truhlar, D. G. Computational Thermochemistry: Scale Factor Databases and Scale Factors for Vibrational Frequencies Obtained from Electronic Model Chemistries. *J. Chem. Theory Comput.* **2010**, *6*, 2872−2887.

(137) Tao, Y.; Zhang, L.; Zou, W.; Kraka, E. Equilibrium Geometries, Adiabatic Excitation Energies and Intrinsic C = C/C-H Bond Strengths of Ethylene in Lowest Singlet Excited States Described by TDDFT. *Symmetry* **2020**, *12*, 1545.

(138) Badger, R. M. A Relation Between Internuclear Distances and Bond Force Constants. *J. Chem. Phys.* **1934**, *2*, 128−131.

(139) Kraka, E.; Larsson, J. A.; Cremer, D. In *Computational Spectroscopy*; Grunenberg, J., Ed.; Wiley: New York, 2010; pp 105−149, DOI: 10.1002/9783527633272.ch4.

(140) Lippert, G.; Hutter, J.; Parrinello, M. A Hybrid Gaussian and Plane Wave Density Functional Scheme. *Mol. Phys.* **1997**, *92*, 477−487.

(141) Kühne, T. D.; Iannuzzi, M.; Ben, M. D.; Rybkin, V. V.; Seewald, P.; Stein, F.; Laino, T.; Khaliullin, R. Z.; Schütt, O.; Schiffmann, F.; Golze, D.; Wilhelm, J.; Chulkov, S.; Bani-Hashemian, M. H.; Weber, V.; Borštnik, U.; Taillefumier, M.; Lazzaro, A.; Pabst, H.; Müller, T.; Guidon, M.; Andermatt, S.; Holmberg, N.; Schenter, G. K.; Hehn, A.; Bussy, A.; Belleflamme, F.; Tabacchi, G.; Glöß, A.; Lass, M.; Bethune, I.; Mundy, C. J.; Plessl, C.; Watkins, M.; VandeVondele, J.; Krack, M.; Hutter, J. CP2K: An Electronic Structure and Molecular Dynamics Software Package - Quickstep: Efficient and Accurate Electronic Structure Calculations. *J. Chem. Phys.* **2020**, *152*, 194103.

(142) VandeVondele, J.; Hutter, J. Gaussian Basis Sets for Accurate Calculations on Molecular Systems in Gas and Condensed Phases. *J. Chem. Phys.* **2007**, *127*, 114105.

(143) Goedecker, S.; Teter, M.; Hutter, J. Separable Dual-Space Gaussian Pseudopotentials. *Phys. Rev. B* **1996**, *54*, 1703−1710.

(144) Hartwigsen, C.; Goedecker, S.; Hutter, J. Relativistic Separable Dual-Space Gaussian Pseudopotentials from H to Rn. *Phys. Rev. B* **1998**, *58*, 3641−3662.

(145) Monkhorst, H. J.; Pack, J. D. Special Points for Brillouin-Zone Integrations. *Phys. Rev. B* **1976**, *13*, 5188.

(146) Vilela Oliveira, D.; Laun, J.; Peintinger, M. F.; Bredow, T. BSSE-Correction Scheme for Consistent Gaussian Basis Sets of Double- and Triple-zeta Valence with Polarization Quality for Solid-State Calculations. *J. Comput. Chem.* **2019**, *40*, 2364−2376.

(147) Dill, J. D.; Pople, J. A. Self-Consistent Molecular Orbital Methods. XV. Extended Gaussian-Type Basis Sets for Lithium, Beryllium, and Boron. *J. Chem. Phys.* **1975**, *62*, 2921−2923.

(148) Hehre, W. J.; Ditchfield, R.; Pople, J. A. Self-Consistent Molecular Orbital Methods. XII. Further Extensions of Gaussian-Type Basis Sets for Use in Molecular Orbital Studies of Organic Molecules. *J. Chem. Phys.* **1972**, *56*, 2257−2261.

(149) Grimme, S.; Ehrlich, S.; Goerigk, L. Effect of the Damping Function in Dispersion Corrected Density Functional Theory. *J. Comput. Chem.* **2011**, *32*, 1456−1465.

(150) Dovesi, R.; Saunders, V. R.; Roetti, C.; Orlando, R.; Zicovich-Wilson, C. M.; Pascale, F.; Civalleri, B.; Doll, K.; Harrison, N. M.; Bush, I. J.; D'Arco, P.; Llunell, M.; Causà, M.; Noël, Y.; Maschio, L.; Erba, A.; Rerat, M.; Casassa, S. *CRYSTAL17 User's Manual*; University of Torino, Torino, 2017.

(151) Csonka, G. I.; Perdew, J. P.; Ruzsinszky, A.; Philipsen, P. H. T.; Lebègue, S.; Paier, J.; Vydrov, O. A.; Ángyán, J. G. Assessing the Performance of Recent Density Functionals for Bulk Solids. *Phys. Rev. B* **2009**, *79*, 155107.

(152) Tao, Y.; Zou, W.; Nanayakkara, S.; Kraka, E. PyVibMS: A PyMOL Plugin for Visualizing Vibrations in Molecules and Solids. *J. Mol. Model.* **2020**, *26*, 290.